Spring 5-15-2020

Influence of Separator Surface Charge on the Nucleation and Penetration Dynamics of Metal Electrodes in Concentrated Electrolytes

Sikuang Wang

Washington University in St. Louis

McKelvey School of Engineering

Department of Energy, Environmental and Chemical Engineering

Influence of Separator Surface Charge on the Nucleation and Penetration Dynamics of Metal Electrodes in Concentrated Electrolytes

By

Sikuang Wang

A thesis presented to the McKelvey School of Engineering of Washington University in St. Louis in partial fulfillment of the requirements for the degree of Master of Science

May 2020

St. Louis, Missouri

Acknowledgements

Special thanks go to Dr. Bai. Dr. Bai supported this research work and spent a lot of time teaching and guiding me through the whole project. Also, thanks go to my thesis defense committee Dr. Jun and Dr. Ramani which help me review and improve this thesis.
Also, thanks go to my family. They support my study mentally and financially.
Mr. James Ballard helped me a lot in improving the writing. Bingyuan Ma, Youngju Lee and Shubham Agrawal helped me in experimental related problems and technical issues.

Table of Contents

List of Tables

List of Figures

Abstract

Influence of Separator Surface Charge on the Nucleation and Penetration Dynamics of Metal Electrodes in Concentrated Electrolytes

By

Sikuang Wang

Master of Science in Chemical Engineering

Washington University in St. Louis, 2020

Research Advisor: Professor Peng Bai

Batteries are ubiquitous in our daily life. However, potential safety issues have hindered the wider market adoption of batteries for other energy storage applications. Developing advanced functional separators that can control and retard safety hazards has become an urgent need. In this thesis work, different types of commercial separators were modified with charged polymers and tested in varouis electrolyte conditions, with a focus on the influence of electrolyte concentration and different pore size on the critical metal penetration capacities. The results suggest in general that negatively charged separators can delay the metal penetration process. Surprisingly, a characteristic current density, i.e. 25% of the system-specific limiting current density, emerged to enable the highest penetration capacity.

Chapter 1: Introduction

1.1 Introduction to battery

The term “battery”, introduced in the mid-18th century, refers to an electrochemical system that converts chemical energy into electrical energy. After hundreds of years of development, common types of batteries have come to include lead-acid batteries, alkaline batteries, redox flow batteries, and lithium ion batteries[2,3].Now, batteries are used everywhere in our life, in cell phones, computers, vehicles, and so on.

1.2 Lithium Ion Batteries and Improvements

The first lithium ion battery was invented in 1970s by Whittingham, Goodenough, Yazami, and Yoshino and was commercialized by Sony in the 1990s [4,21]. In recent years, more and more electronic devices use Lithium ion battery as their power source even the large electric vehicle use Lithium ion battery to drive the motors. In general, electric cars share the same type of power source as our cell phones [13]. Fig.1 show that lithium ion batteries have relatively high energy density and an output of more than 3V [5]. Now, lithium ion batteries are the primary choice for the most of electronic devices such as cell phones, laptops, electric vehicles and so on. With increasing performance of all electrical devices, the lithium ion batteries are expected to have higher energy density and be safe. For example, the Tesla Model S P100D has the highest capacity among all the models but only has 315 miles range but the battery pack has weight more than 600 kg.

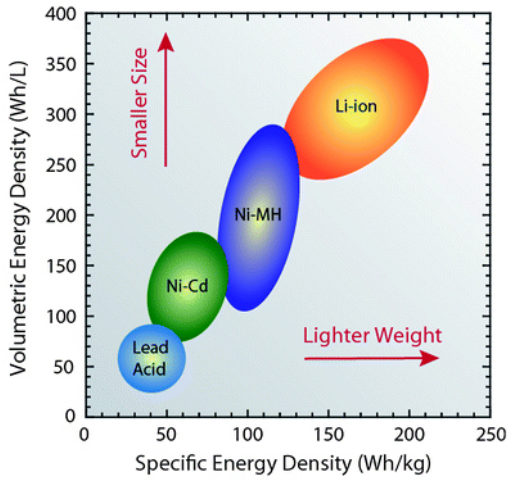

Figure 1 Energy density of batteries.

In order to increase the energy density of Lithium ion battery, the structure of Lithium ion battery can be modified. Commonly, lithium ions will be reduced into graphite as the anode material. If we remove the anode material and let lithium directly be reduced on the anode surface as shown in the Fig. 2, we can save considerable proportion of space and weight so that the energy density of the battery increases. This design does present a problem in operation. As the lithium ions are reduced directly on the surface of the anode, dendrites or whiskers will be formed. These dendrites can penetrate the separator in the batteries and resulting an inner short circuit that overheats the battery and causes it to catch fire. To fundamentally improve the design of the lithium ion battery, separator penetration must be suppressed.

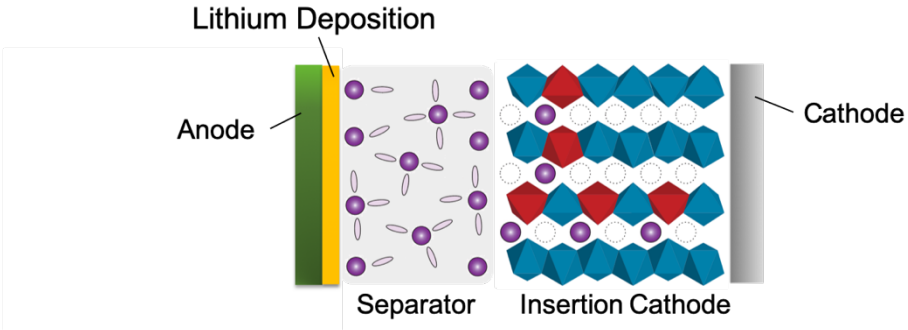

Figure 2 Battery with anode removed structure

Chapter 2: Research Motivative and Hypothesis

From previous work, the surface charge effect had been discovered. The different charges on the pores will have higher concentration of either cation or anion at their double layer. The difference between positively charged and negatively charged separators can influent the transportation through the pores so that affect performance, and that result in the different between limiting current and over-limiting current [8,9]. Over-limiting current is defined as current is larger than the diffusion limitation and is possibly caused by mass transfer mechanisms other than electro-diffusion or electrochemical reactions [6,7]. According to the result from 2014, at low concentration, negatively charged separators show over-limiting current performance and positively charged separators didn't show the phenomenon [8]. During the deposition process, different surface charge will result in different mechanisms. For positively charged separators, the double layer will have higher concentration of anion and negatively charged separator will have higher concentration of cation at the double layer. When depletion happened, the cation will be reduced into metal and left depletion region near the anode. The negatively charged pores can enhance the cation supply due to the electrostatic force between negatively charged pores and cation. But positively charged pores will only have cation channel in the middle. For positively charged separators, the dendrite will grow only in center of the pore and left the deposition into a transport limitation process to slow down the growth of the dendrite, so that ensure the safety. For negatively charged separators, the dendrite will grow along the pores and the growth will be accelerated due to surface charge effect [10,11,12]. The surface charged effect is expected to be affect by double layer to radius ratio which affect by both concentration and pore size. Ceramic coated separators, Polypropylene-Polyethylene-Polypropylene (tri-layer PE) separators and cellulose nitrate separators were chosen to be tested.

Chapter 3: Experiments Preparation and Setup

3.1 Separators

Ceramic coated, Tri-layer PE and cellulose nitrate separators are used. Ceramic coated and tri-layer PE separators are from MTI corp. Cellulose nitrate separators are from GE HealthScience. The specifications of these separators are summarized in the table below.

Separator\Specs	Thickness (μm)	Porosity	Tortuosity	Pore Size (nm)
Ceramic coated	16	0.39	3.43	26
Tri-layer PE	25	0.4	2.23	PE:26 / PP: 50
Cellulose Nitrate	200	0.66	1	200

Table 1. Separators specification.

3.2 Plasma Treatment

Plasma cleaning process is also called plasma treatment and it is essential to the separator's preparation. During the plasma treatment, the particle from the surface of the separators can be removed and the separators are negatively charged. Also, the wettability of the separators because the ceramic coated and tri-layer PE separators have bad wettability before any treatment [14, 15]. The plasma is generated in the chamber of plasma cleaning machines. Normally, the pressure inside of the chamber is kept around 760mTorr [14,15]. The plasma is in pink to rose red color if the pressure is well maintained. For different types of separators due to differences on the material property. Ceramic coated needs seven mins to clean one side. Cellulose nitrate needs 60 seconds for each side. Tri-layer PE needs eight mins to clean for each side. Plasma

cleaning machines will generate a considerable amount of heat in the chamber during the cleaning process. The temperature could rise to more than 80 degree Celsius. In order to avoid melting down or deformation during the plasma treatment, the tri-layer PE separators will be treated two four-minute treatment with 3-minute cooling down between them. After both sides of the separators are done with plasma treatment, the separators are soaked into the prepared polyelectrolyte solution immediately.

3.3 Polyelectrolyte Solution

PDADMAC (poly(diallyldimethlyammonium chloride)) and PSS (poly(styrene sulfonate)) are the two polyelectrolyte that are made separators charged. PDADMAC is the polymer chloride salt and the polymer will indicate positively charged after dissolved.

To prepare PDAMAC solution, 200mM of sodium chloride solution is made first. Then we add PDADMAC (high viscosity liquid with Mw around 200,000-350,000) following the ratio of 2.5ml PDADMAC: 500 ml sodium chloride solution and put the bottle into the water bath sonicator for 10 mins. PSS solution is prepared with similar procedure. We add PSS (white powder with Mw around 70,000) into the sodium chloride solution with ratio 1mg PSS: 1ml sodium chloride solution, then sonicate for 10 mins.

3.4 Layer-by-layer assembly

Positively charged separators are prepared by soaking the plasma treated separators into the positive polyelectrolyte solution (PDADMAC solution). The positive polyelectrolyte absorbed on surface. After soaking for one hour, taking out the separators and soaking that again

with DI water for one hour to clean the residual polyelectrolyte. To make the negatively charged separators, taking out cleaned positively charged separators and soaking into negative polyelectrolyte solution (PSS). Positively charged and negatively charged layer-by-layer structure is shown in Fig 3. After cleaning with DI water, the negatively charged separators are ready to use [18,19,20].

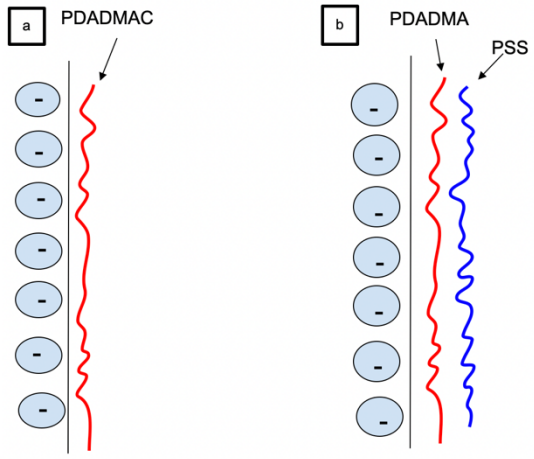

Figure 3 1

Figure 3 Layer-by-Layer structure. (a) positively charged. (b) negatively charged

3.5 Testing cell assembly

The testing cells for LSV and chronopotentiometry are assembled as the figure shown below(figure2,3). The testing cell is in the symmetrical structure. Copper electrodes are cut from copper plates with a square shape of 1.4 cm by 1.4 cm. Two copper electrodes are separated by one layer of separator (SEM sample have washer and copper foil between electrode and separator). For copper each electrode, the side facing to the separators will be polished to mirror finish with the fine sandpaper to make a flat and smooth surface. Another side will be sealed

with hot glue. The wire will connect to the sealed side of the copper electrode. The whole cell is soaked into copper sulfate solution in the beaker with parafilm covered during all tests. The tests are done in copper sulfate aqueous solution instead of non-aqueous Lithium battery system. This system is not sensitive to oxygen and moisture, furthermore, there is no solid electrolyte interphase in copper sulfate system [22].

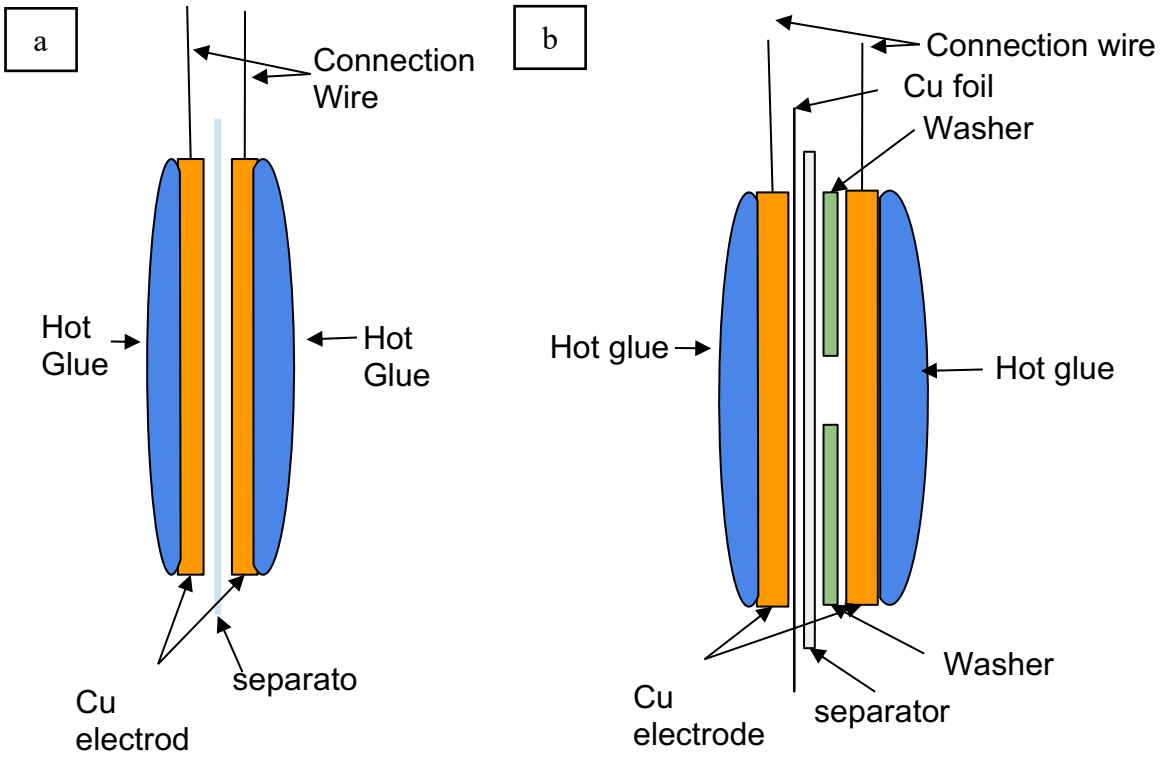

Figure 4 Test cell structure. (a) normal test cell. (b) SEM sample preparation test cell.

Chapter 4: Results and Discussions

4.1 Linear Sweep voltammetry

In Ji-Hyung's paper, the symmetric copper cell was only tested in the extreme diluted copper sulfate solution (75mM) and separator performance at high concentration is briefly mentioned as surface conduction effect disappeared [8]. In the commercial batteries, the concentration of electrolyte is around 1M considered as optimum. In this part, symmetric cells are tested in a variety of concentrations.

In the linear sweep voltammetry test, positively charged separators are expected to have limiting current response and negatively charged separators are expected to have over-limiting current response due to the surface charge effect. The theoretical value of limiting current is defined as the equation below.

$$I_{lim} = \frac{4ze\varepsilon_p DA}{\tau L} {C_0}^{\infty} \text{ [8]}$$

And limiting current density for each separator and concentration had been summarized in the table 2. 100mM, 250mM, 500mM and 1M concentration of copper sulfate solution is used to test all three types of separators with both positive and negative charges.

Separator\Concentration	100mM	250mM	500mM	1M
Ceramic coated	$0.0010 A/cm^2$	$0.0251 A/cm^2$	$0.0502 A/cm^2$	$0.1004 A/cm^2$
Tri-layer PE	$0.0095 A/cm^2$	$0.0238 A/cm^2$	$0.0476 A/cm^2$	$0.0951 A/cm^2$
Cellulose Nitrate	$0.0045 A/cm^2$	$0.0113 A/cm^2$	$0.0227 A/cm^2$	$0.0005 mA/cm^2$

Table 2. Limiting current density table.

As result shown in the figure 5 and 6, for low concentration 100mM and 250mM, all separators show the same response at low voltage from 0 to 0.1 V. And from 0.1 to 0.2 V, the curves increase monotonically with voltage increases. After 0.2V, the potential of the system is high enough so that diffusion limitation leads the limiting current plateau to show up. For all positively charged ceramic coated, tri-layer PE and cellulose nitrate separators, plateaus are obvious and uniform. For all negatively charged separators, over-limiting current response is observed after 0.2V.

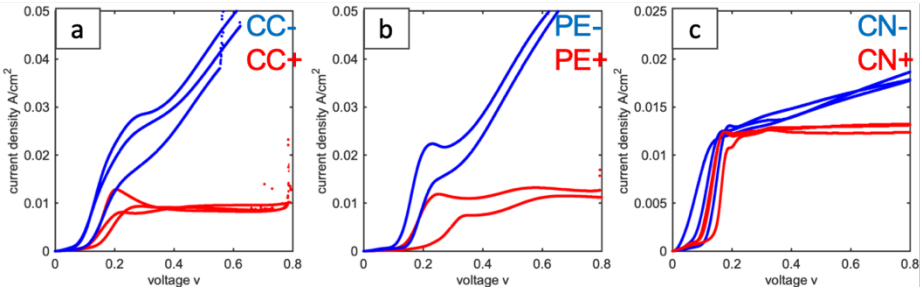

Figure 5 Linear Sweep Voltammetry result in 100mM copper sulfate. (a) ceramic coated. (b) Tri-layer PE. (c) cellulose nitrate.

By comparing the curves for positively charged and negatively charged separators, the difference is large for all types of separators. When concentration rises to 250mM, the difference between positively charged and negatively charged cellulose nitrate separators show smaller differences than theirs in the 100mM concentration.

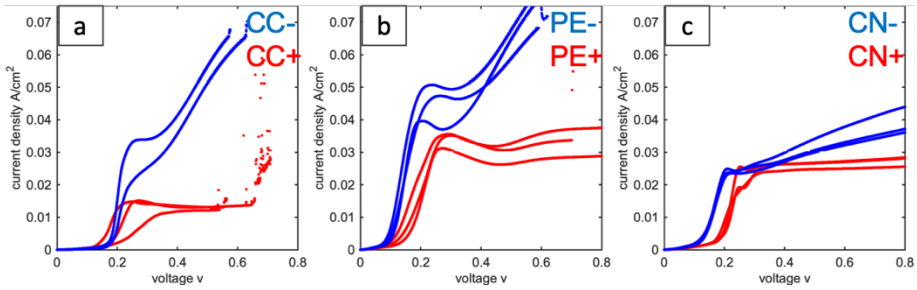

Figure 6 Linear Sweep Voltammetry result in 250mM copper sulfate. (a) ceramic coated. (b) Tri-layer PE. (c) cellulose nitrate.

The figure 7 shows that when concentration increases to 500mM, the differences between positively charged and negatively charged tri-layer PE and cellulose nitrate separators become smaller and smaller. Especially for cellulose nitrate separators, the differences are ignorable. Both positively charged and negatively charged separators have almost overlapped curves until 0.2V. After 0.4V, all curves increase monotonically, and the slope of the curves is almost the same and negatively charged separators have slightly higher current response. At this concentration, the surface charge effect in the cellulose nitrate separators is very weak. Since the cellulose nitrate separators have the largest pores size (around 200 nm) and the double layer to radius ratio is the largest among three types of the separators. We can conclude that the surface charge effect in the large pores is reduced when concentration rise.

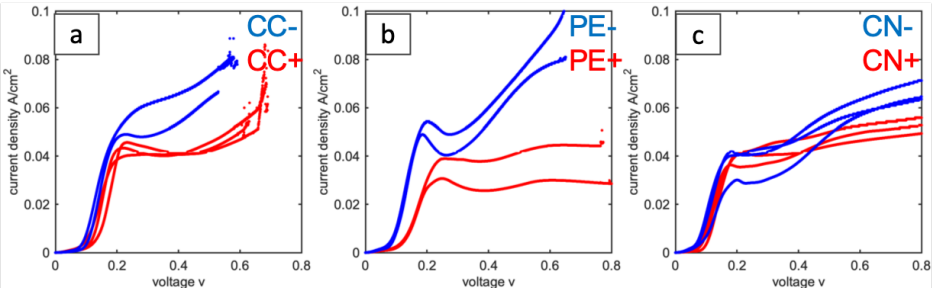

Figure 7 Linear Sweep Voltammetry result in 500mM copper sulfate. (a) ceramic coated. (b) Tri-layer PE. (c) cellulose nitrate.

When concentration is raised to 1M, except ceramic coated separators, the difference between positively charged and negatively charged separators become smaller and smaller. For cellulose nitrate separators, the difference is minimized. Curves for positively charged and negatively charged separators are overlapped. The phenomenon indicates that the surface conduction effect disappeared in the cellulose nitrate system at high concentration. For tri-layer PE separators, the curvatures look alike, and we can conclude that the surface conduction effect is also reduced in the tri-layer separators in the high concentration system. Only ceramic coated

separators still show the significant difference between positively charged and negatively charged separators. By comparing the size of the pores for ceramic coated separators and tri-layer PE separators, tri-layer PE separators have smaller double layer to radius ratio than ceramic coated separators and we can conclude that surface charge effect is still significant in the ceramic coated separators.

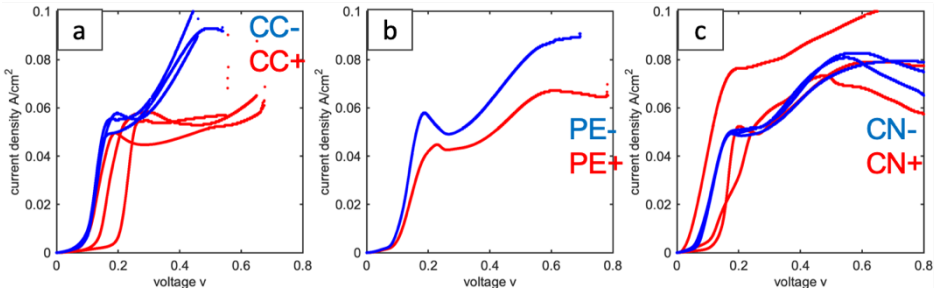

Figure 8 Linear Sweep Voltammetry result in 1M copper sulfate. (a) ceramic coated. (b) Tri-layer PE. (c) cellulose nitrate.

By comparing the theoretical current density and experimental current density, all experimental results are within the same magnitude of theoretical calculations. Surface conduction effect is correlated with double layer to radius ratio which is consistent with our hypothesis. When the pore is large, the small double layer to radius ratio results in the weak surface charge effect. Also, concentration of electrolyte will also affect the surface charge effect. When the concentration increases, the Debye length decreases. And the surface charge effect is also reduced because of small double layer to radius ratio. For example, the Debye length for 10mM copper sulfate solution is 4.8 nm and the Debye length for 100mM copper sulfate solution is 1.52nm which is considerably smaller than previous value. Ceramic coated separators have the smallest pore size among three types of separator and have the highest double layer to radius ratio, so that the surface charge effect can be still observed at concentration electrolyte.

4.2 Chronopotentiometry

By comparing the performance of positively charged and negatively charged separators, we can observe that the negatively charged separators systems can be pushed to over-limiting current regions. But in reality, no battery can or will work in the over-limiting region. In order to determine the performance for both positively charged and negatively charged separators in real-life usage, we mimic the condition in the battery to do the chronopotentiometry. We recorded the limiting current at 1M for each type of separators and tested with 5% 10%, 25% and 50% of theirs limiting current. Separator penetration is defined as voltage sudden drop.

At a low percentage of limiting current shown in figure 9, all types of separators show that positively charged separators have higher voltage response than negatively charged ones. From another point of view, positively charged separators need higher potential to reach the same current. And in general, negatively charged separators have a higher chance to sustain longer before penetration happens compared with positively charged ones. Especially for ceramic coated separators, negatively charged separators can sustain almost two times longer than positively charged ones. For tri-layer PE and cellulose nitrate separators, negatively charged are slightly better than positively charged ones.

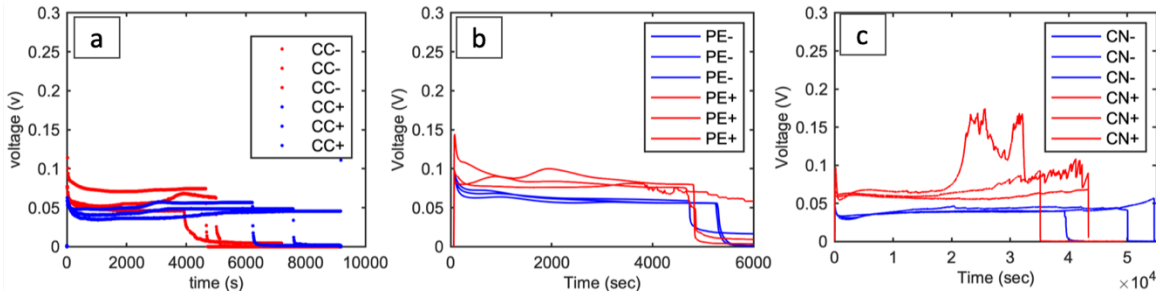

Figure 9 Chronopotentiometry result at 5% limiting current. (a) ceramic coated. (b) Tri-layer PE. (c) cellulose nitrate.

The results in figure 10 show the chronopotentiometry at 10% limiting current. All three types of separators show that negatively charged separators could resist the penetration longer. Also, positively charged separators will have higher voltage response than negatively charged separators.

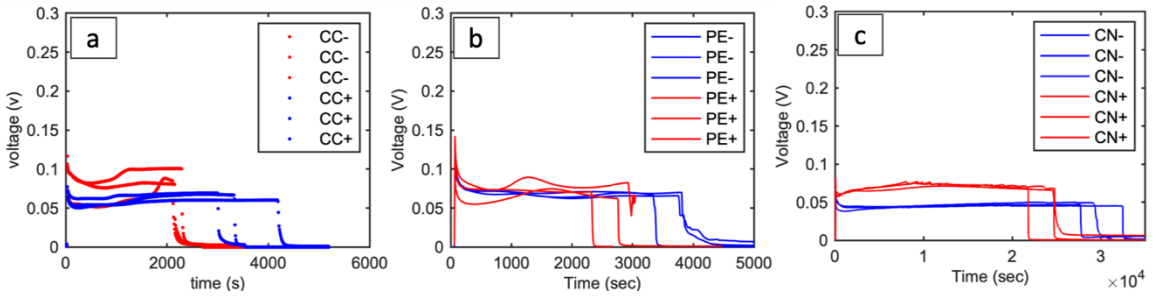

Figure 10 Chronopotentiometry result at 10% limiting current. (a) ceramic coated. (b) Tri-layer PE. (c) cellulose nitrate.

When the percentage of limiting current rises to 25% of their limiting currents (shown in figure 11), positively charged and negatively charged cellulose nitrate separators have no performance difference. Positively and negatively charged ceramic coated and tri-layer PE show small performance differences even though negatively charged separators can still sustain longer time.

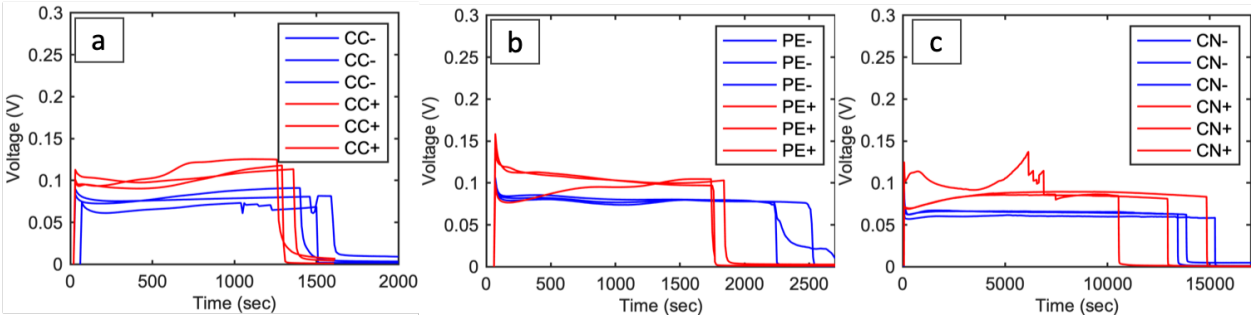

Figure 11 Chronopotentiometry result at 25% limiting current. (a) ceramic coated. (b) Tri-layer PE. (c) cellulose nitrate.

For 50% of limiting current, all types of positively and negatively charged separators are likely to be penetrated at similar time. Also, the voltage response difference between positively charged and negatively charged separators are totally negligible for all separators.

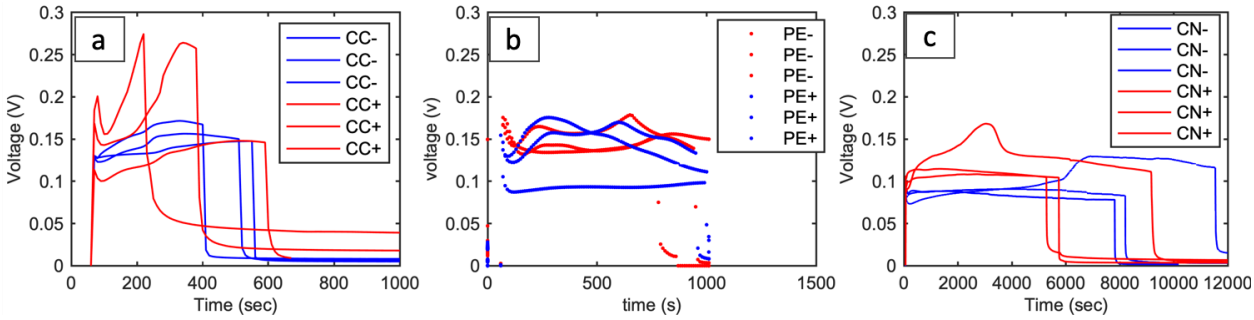

Figure 12 Chronopotentiometry result at 50% limiting current. (a) ceramic coated. (b) Tri-layer PE. (c) cellulose nitrate.

If we only consider the performance differences between positively charged and negatively charged separators, in general, we can conclude that, negatively charged separators have a higher chance to have better performance than the positively charged separators in low percentage (less than 10%) of their limiting current. When the percentage of their limiting current is high, both positively charged and negatively charged separators have almost the same performance. In order to compare the performance of the separators in different percentages of limiting current, the statistics is done to show the details in figure 13.

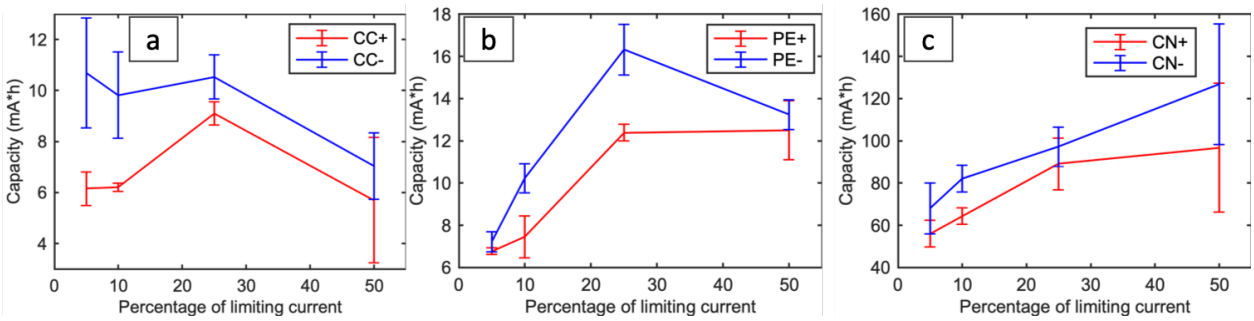

Figure 13 Penetration capacity statistics. (a) ceramic coated. (b) Tri-layer PE. (c) cellulose nitrate.

By comparing the penetration capacities of ceramic coated, tri-layer PE and cellulose nitrate separators, we can tell that cellulose nitrate separators have the highest penetration capacities due to the thickness. Cellulose nitrate separators have the highest thickness among these three types of separators. And penetration capacities are proportional to the thickness which is logically making sense. In addition, there are some interesting points in the statistical graph.

First, for ceramic coated separators, both positively and negatively charged penetration capacities curve are non-monotonic. In the graph, the penetration capacity difference between positively charged and negatively charged separators is very large at a low percentage of limiting current (LC). With the percentage of limiting current increases, the difference becomes smaller and smaller. At 25% of LC or higher, the penetration capacity difference is almost the same. Furthermore, we can tell that negatively charged separators are likely to have the highest penetration capacity at 25% of LC and positively charged separators have the highest penetration capacity at 25% of LC. In general, penetration capacities for negatively charged separators are larger than penetration capacities for positively charged separators at all range of current density.

For tri-layer PE separators, negatively charged separators have better performance than positively charged ones among all percentages of LC. At 5% of LC, positively charged and negatively charged separators show similar performance on penetration capacities. With the percentage of LC increases from 5% to 25%, the difference between positively charged separators and negatively charged ones becomes larger and larger. The largest difference is reached at 25% limiting current. For 50% of LC, the performance difference between two types of separators are very small. In general, both positively charged separators and negatively charged separators show the monotonic growth of penetration capacities from 5% to 25% LC.

When the percentage of limiting current increases from 25% to 50%, the penetration capacities drop for both positively charged and negatively charged separators. Negatively charged separators indicate that 25% of LC will have the optimum penetration capacities. Positively charged separators indicate that 25% of LC will possibly have the highest penetration capacity.

For cellulose nitrate separators, negatively charged separators have higher penetration capacities than positively charged separators in the all four-percentage limiting current we tested. Compared with ceramic coated and tri-layer separators, the penetration capacities vs limiting current curves are different. Both curves are monotonically increasing with a percentage of limiting current.

4.3 Scanning Electron Microscopy (SEM) Characterization

In order to understand the causes to have different penetration capacities curves, SEM images are taken after each test. The SEM scanning is focusing on two parts, the penetrated part and unpenetrated part, as schematically demonstrated in Fig. 14.

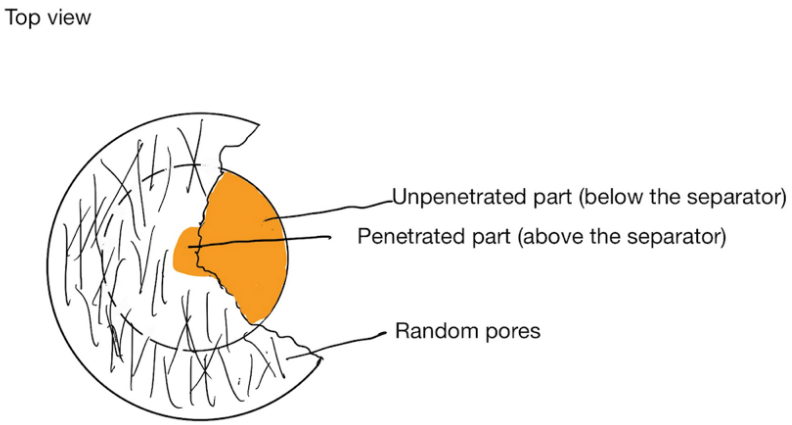

Figure 14 Top view of SEM image indication.

For each sample, 250X, 1,000X and 10,000X images are taken in order to compare the macroscale and microscale of the deposition morphology. To better reveal the details of the deposition morphology, relatively large size of the SEM images was used. The images from each sample, i.e. same type and same control parameters, but characterized at three different magnifications were group into one figure. To ensure easy reading of the text and the corresponding figures, all figures are appended after the text of this chapter.

For negatively charged ceramic coated separators, the local high penetration capacity is likely reached at 25% of LC. In the underneath SEM images, the 10% LC figure (Fig. 14 (a)) shows the relatively large nucleation; the 25% LC figure (Fig. 15(a)) shows smaller and more compact nucleation; the 50% LC figure (Fig. 16(a)) shows more spherical and more compact nucleation just like small particles grow into the whole pack. Fig. 14(c) shows the 10k magnification, the 10% LC sample has the largest nucleation size and the tiny nucleation sites show up randomly on the large nucleation surface. Fig. 15(c), the 25% of LC sample shows smaller nucleation size. And the distance between each nucleation site is larger than 10% of LC ones. Small nucleation sites are observed on the edge of the large nucleation crystal structure only. Fig.16 (c) shows the 50% LC sample have the nucleation sites distance is close to 25% LC sample. The small nucleation sites found on the surface of the large crystal like the 10% LC sample, but the large nucleation crystals are not in regular shape compared with the 10%LC sample. For the penetrated part, we can observe similar morphology with the underneath part. Fig. 17(a), Fig. 18(a) and Fig. 19(a) show that 10% LC sample has the small and loose nucleation crystals and 25% or 50% LC samples have large and more compact nucleation crystals than 5% of LC sample. Fig. 17(c), Fig. 18(c) and Fig. 19(c) show the nucleation distance of 10% LC sample is larger than 25% and 50% LC samples. On the surface of large nucleation

crystals, small random nucleation sites are observed for the 10% LC sample. The 25% LC sample has almost no small nucleation sites. The 50% LC sample has nucleation sites only on the edges.

For negatively charged tri-layer PE, the local high penetration capacity is observed from the statistics graph which is similar with positively charged ceramic coated separators. Logically, the nucleation morphology should be similar. Fig. 20(b) and Fig. 22(b) indicate the 10% LC and 50% LC samples' compact structure. Fig. 21(b) shows 25% LC sample's structure looks like a lot of individual crystal stack side by side. Fig. 20(c) and Fig. 22(c) At higher magnification, we can tell that the nucleation distance for 10% LC and 50% LC samples varies in a large range and are hard to measure due to the rough surface. Figure. 21(c) shows that 25% LC sample has more regular nucleation distance. In contrast, the 10% LC and 50% LC samples show irregular, broken nucleation crystals. The 10% LC sample has a few small nucleation sites on the surface. The 25% LC and 50% LC samples have a lot of small nucleation on the edge of the large nucleation crystal. Clearly, a 25% LC sample has a more flat and large nucleation crystal than the 50% LC sample.

For the penetrated part show in Fig. 23(a), Fig. 24(a) and Fig. 25(a), all samples show small and compact nucleation. The 10% LC sample shows some large nucleation crystals in part of the figure might be due to the high local high current density. The 25% LC sample shows more compact for the whole picture and more uniform for each nucleation crystal. The 50% LC sample shows the spherical shape nucleation crystal. The size of crystal varies in a large range comparing the top and bottom in the figure. Fig. 23(c) show the 10%LC sample has small nucleation distance (around 20 microns). Fig. 24(c) and Fig. 25(c) The 25% LC sample and 50% LC sample have nucleation distance about 40 and 50 microns. The 10% LC and 50% LC

samples have small nucleation sites randomly distributed on the surface. The 25% LC sample has a tiny nucleation site on the surface of a small nucleation crystal. The large nucleation crystal is relatively flat and smooth.

For the cellulose nitrate separators, penetration capacities grow with a percentage of limiting current increases. For underneath part of negatively charged separators, Fig. 26(a), Fig. 27(a) and Fig. 28(a), compact structure observed for all percent of limiting current. Fig. 27(b) and 28(b) show the 25% LC sample shows that nucleation sites are larger than background ones and the 50% LC samples show nucleation sites growing into a large one. Fig. 26(c) and Fig. 27(c) show the 10% LC sample shows small nucleation sites randomly found on the surface at microscale and the 25% LC sample has less small nucleation sites. Fig. 28(c) show the 50% LC sample shows the blooming small random nucleation sites on the surface. For the penetrated part, we can clearly tell that with the percentage of limiting current increases, the nucleation size and nucleation distance becomes larger and larger.

For positively charged ceramic coated separators, the local high penetration capacity is reached at 25% LC. Fig. 32(a), Fig. 33(a) and Fig. 34(a) show that all underneath samples show very small and compact deposition. The 25% LC sample has the flattest deposition than 10% LC and 50% LC samples. All samples indicate the packed deposition. Down to 10K scale, Fig. 32(c), Fig. 33(c) and Fig. 34(c) show the 10% LC sample has the largest nucleation separation distance and 25% LC and 50% LC samples have similar nucleation distance. The 10% and 50% LC samples have small nucleation sites randomly. The 25% LC has relatively small nucleation crystal size, but small nucleation sites only observed on the edge of surfaces. Furthermore, the nucleation crystals in 25% LC are more likely in the same height. The nucleation crystals in 10% and 50% LC samples are not in the regular shape compared with 25% LC one. Similar result is

observed in Fig.35, Fig. 36 and Fig. 37. The 25% LC sample show the more regular crystal and smoother surface.

For positively charged tri-layer PE, the 25% LC and 50% LC tests have similar penetration capacities. Fig. 39(a) and Fig. 40(a) indicate the structure of 25% LC and 50 LC samples are expected to be similar. Fig.38(c), Fig. 39(a) and Fig. 40(a) show the underneath part of 10% LC sample had very large crystals compared with 25% LC and 50% LC samples. For Fig. 38(b), Fig. 39(b) and Fig. 40(b), we can see both 25% LC sample and 50 % LC sample show the compact nucleation crystal structure. The 10% LC sample shows that only a few large nucleation sites. Furthermore, the 10% LC shows the very rough and irregular surface. For 25% LC and 50% LC samples, the nucleation sites compact together. The 50% LC sample has irregular broken nucleation structure with a small nucleation site randomly found. The 25% LC sample has more side by side compact nucleation instead of covering style nucleation and the small nucleation sites are widely spread on the surface. Turning to the penetrated part, Fig. 41(a) show that the 10% LC sample shows small and chaotic nucleation structure. From Fig. 42(a) and Fig. 43(a), the 25% LC and 50% LC samples show more spherical and more regular shape. The 10% LC sample shows small nucleation distance around 5 microns and the small nucleation sites are found randomly on the surface. Fig. 42(b) show the 25% LC samples show the large nucleation distance between 80 to 100 microns and large nucleation size more than 100 microns in average. Fig. 42(c) shows the rough and broken surface of the large nucleation crystal. The 50% LC sample shows nucleation distance around 20 microns with regular nucleation structure and the small nucleation crystals are observed growing on the big nucleation sites from Fig. 43(c).

For positively charged cellulose nitrate separators with underneath part shown in Fig. 44(a),), Fig. 45(a) and Fig. 46(a), the morphology of the nucleation is quite similar with negatively charged cellulose nitrate separators. Fig. 44(b),), Fig. 45(b) and Fig. 46(b) show that all samples are all in packed shape and some small nucleation sites grew on the top of the large surface of nucleation. Fig. 44(c) and Fig. 45(c) show the 10% LC sample shows larger nucleation sites on the surface than the 25% LC sample did. The 50% LC sample has the smallest nucleation sites on the surface from Fig. 46(c). In general, the nucleation size decreases as the percentage of limiting current density increases.

For penetrated part of positively charged cellulose nitrate separators, we observed completely different morphology from Fig. 47(b), Fig. 48(b) and Fig. 49(b). With the percentage of limiting current density increases, the nucleation crystal size increases. Fig. 47(c), Fig. 48(c) and Fig. 49(c) show the surface morphology at high magnification is almost identical to what we observed in negatively charged separators.

In general, the optimum penetration capacities happen when deposition on the electrode have more regular nucleation structure and secondary nucleation sites on the surface of large nucleation crystals grow on the edge only instead of randomly distributed on the surface. The nucleation size did not play an important role for identifying performance of the penetration capacity. For ceramic coated separators and tri-layer PE separators, the 25% LC trend to have the smooth, regular and uniform nucleation structure then another percentage of limiting current.

a

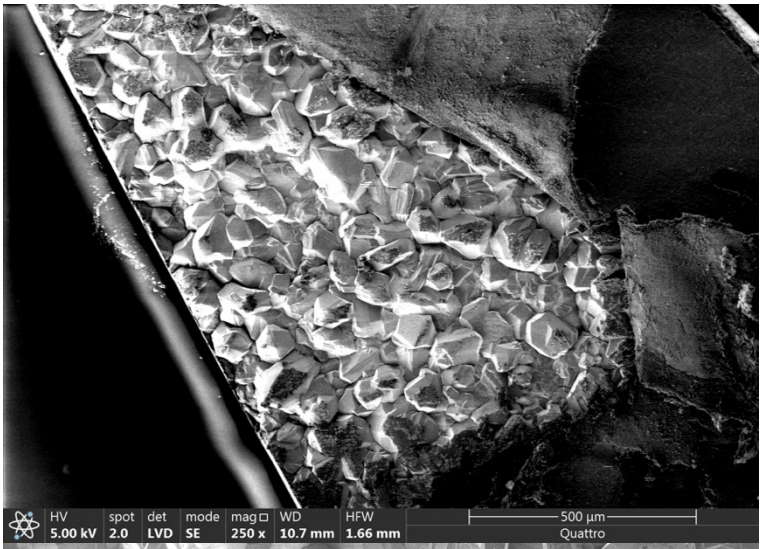

b

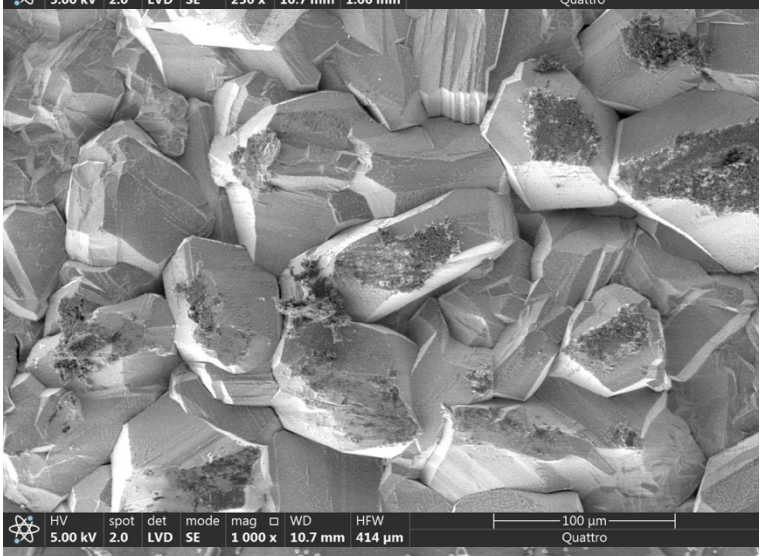

c

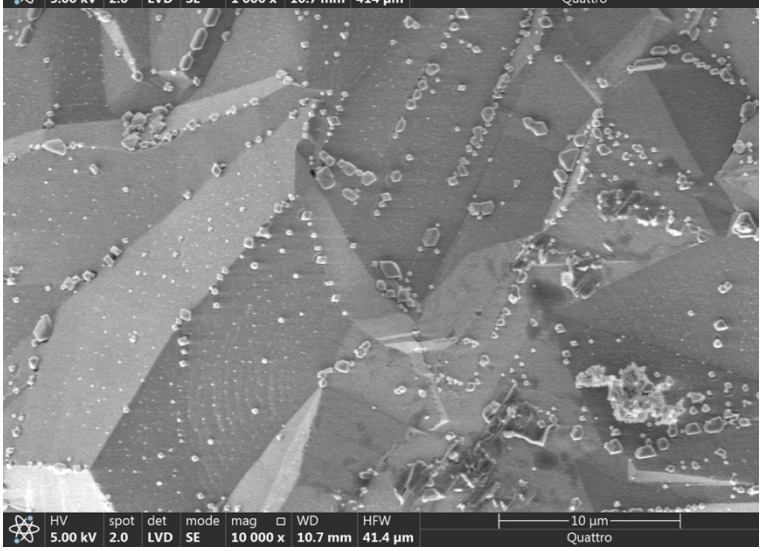

Figure 15 SEM images of unpenetrated part of negatively charged ceramic coated at 10% of limiting current. (a) 250X. (b) 1000X. (c) 10,000X. Please refer to Fig.10(a) for the electrochemical method to obtain this sample

a

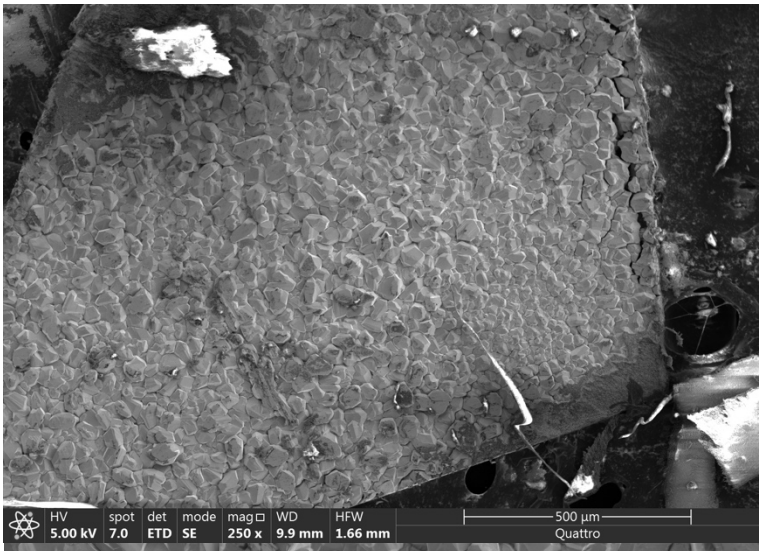

b

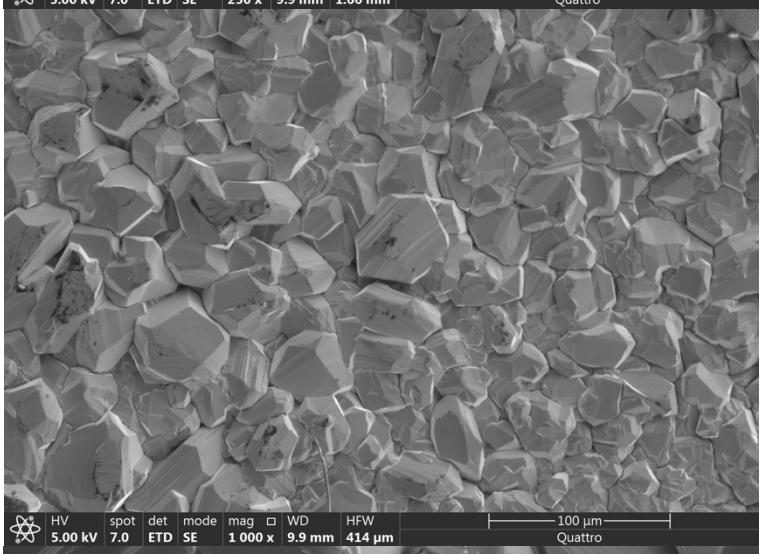

c

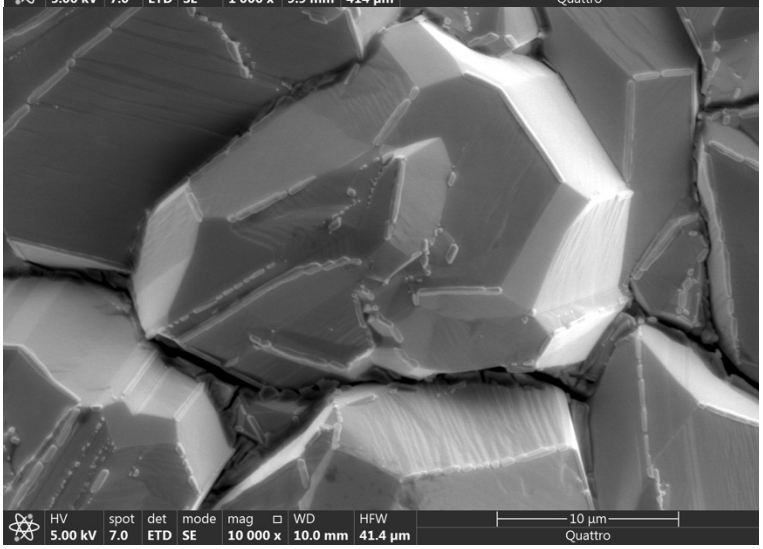

Figure 16 SEM images of unpenetrated part of negatively charged ceramic coated at 25% of limiting current. (a) 250X. (b) 1000X. (c) 10,000X. Please refer to Fig.10(a) for the electrochemical method to obtain this sample

a

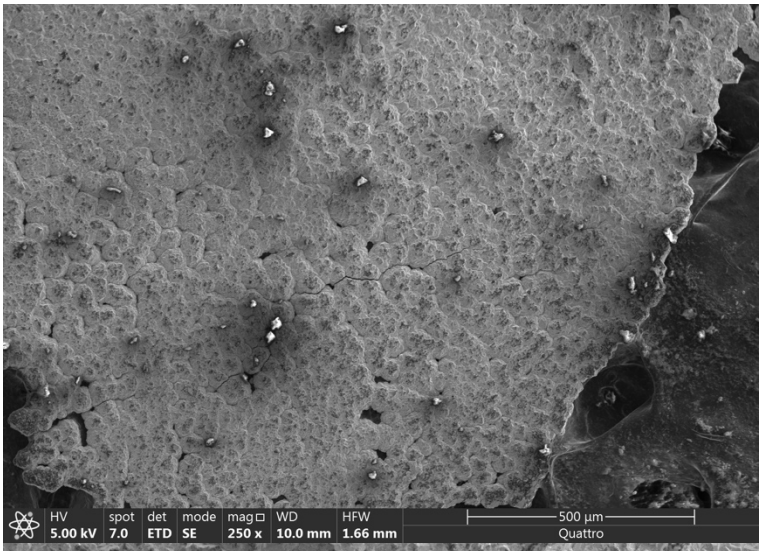

b

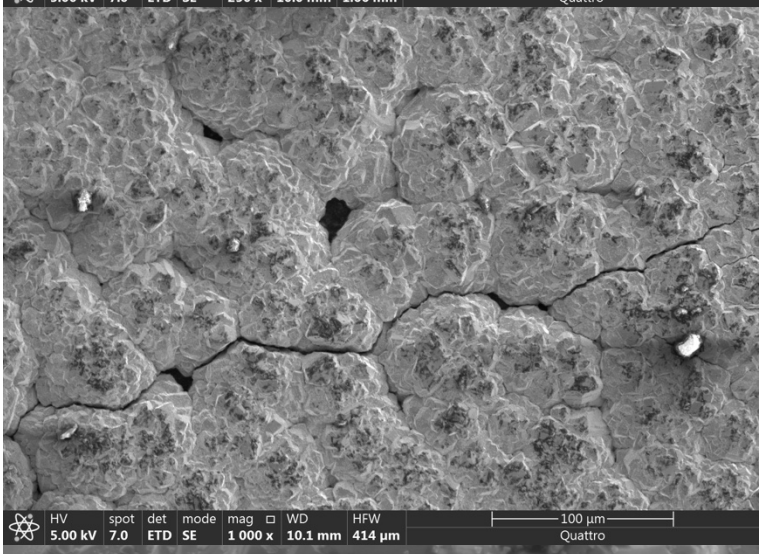

c

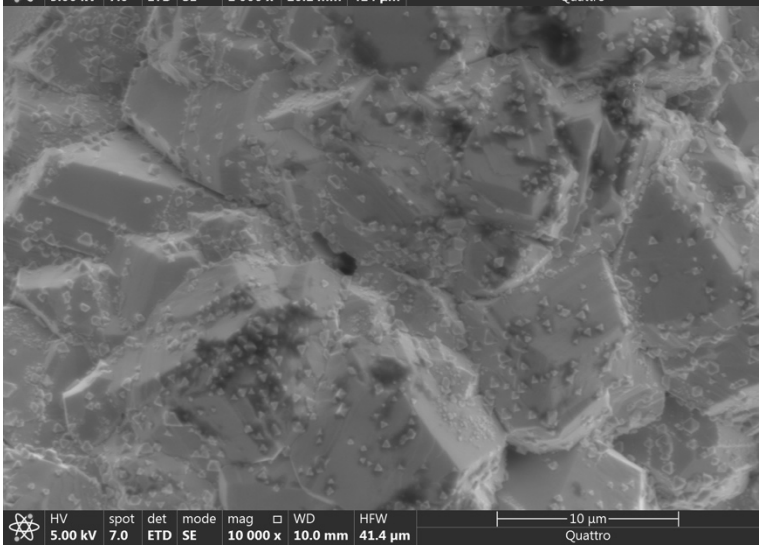

Figure 17 SEM images of unpenetrated part of negatively charged ceramic coated at 50% of limiting current. (a) 250X. (b) 1000X. (c) 10,000X. Please refer to Fig.11(a) for the electrochemical method to obtain this sample

a

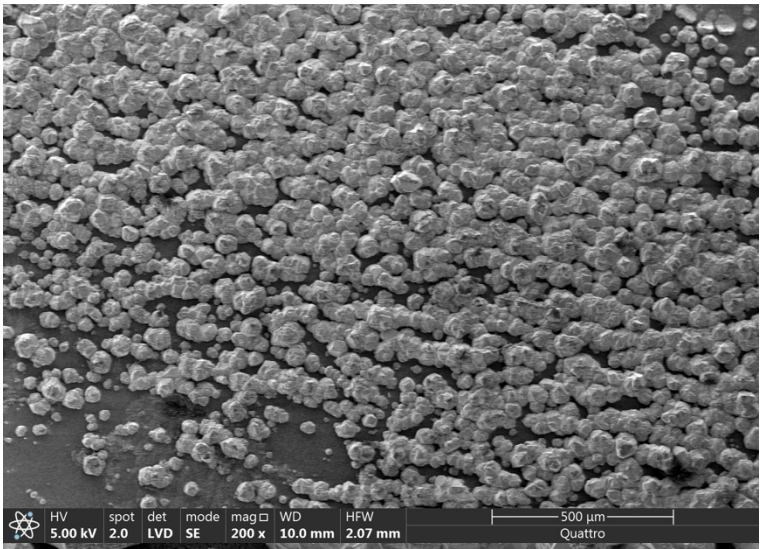

b

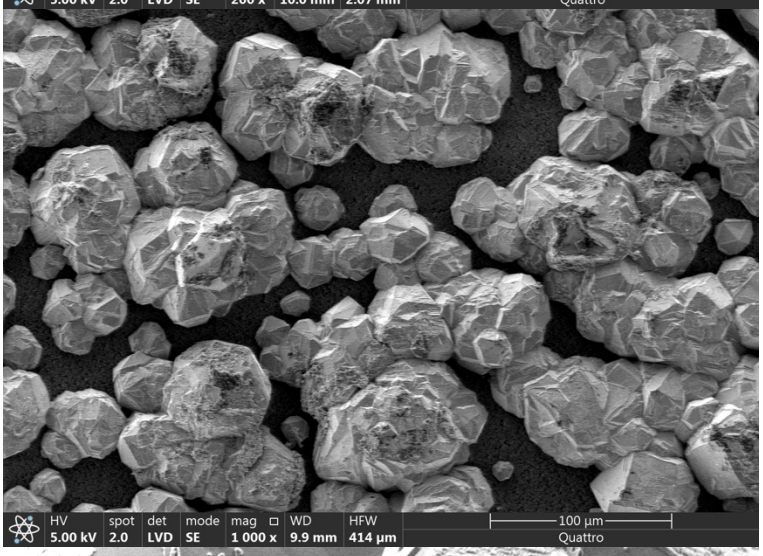

c

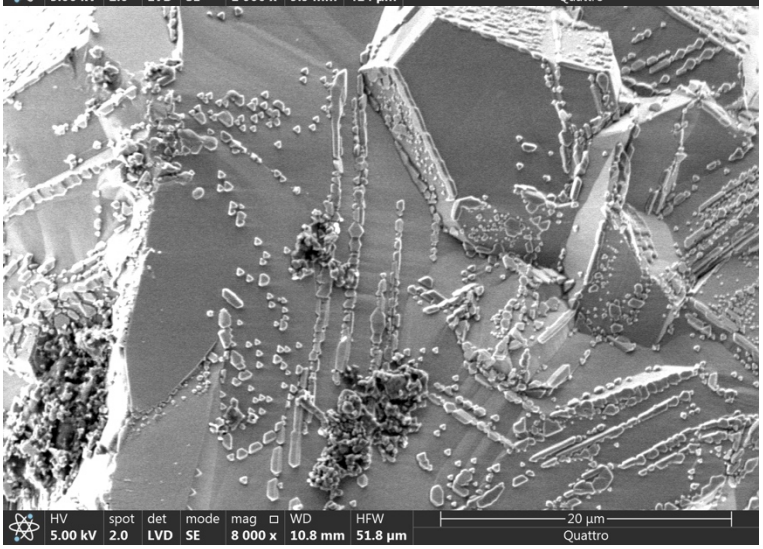

Figure 18 SEM images of penetrated part of negatively charged ceramic coated at 10% of limiting current. (a) 250X. (b) 1000X. (c) 10,000X. Please refer to Fig.10(a) for the electrochemical method to obtain this sample

a

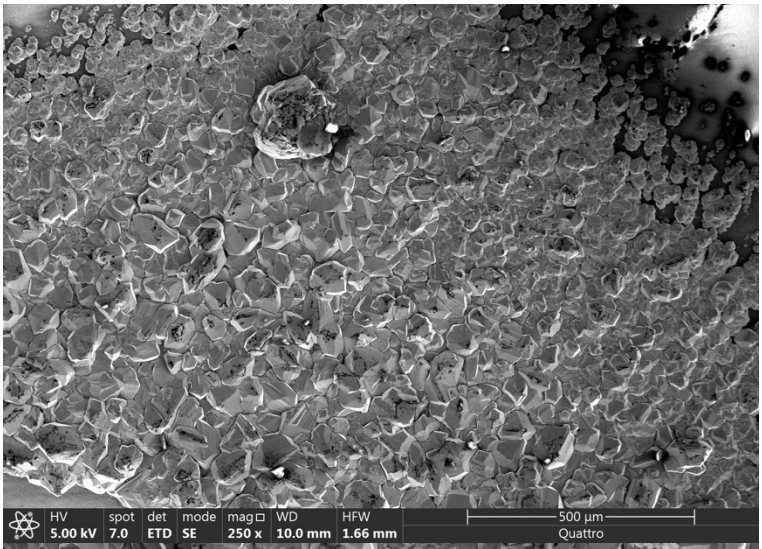

b

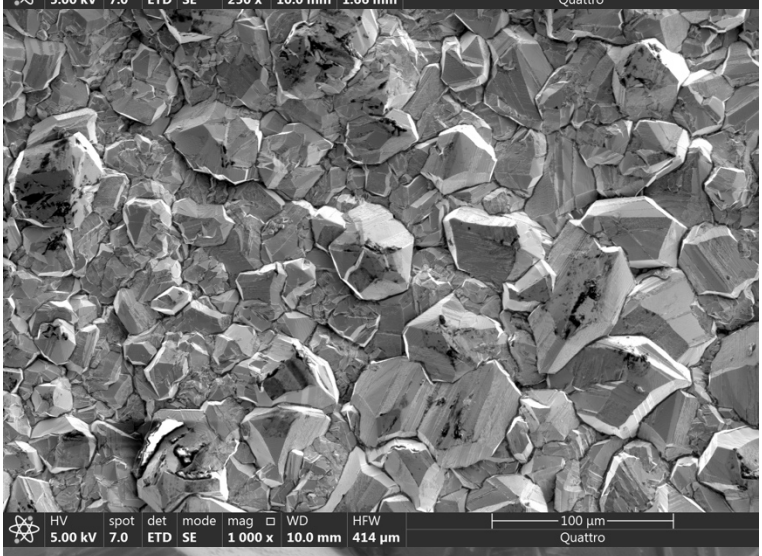

c

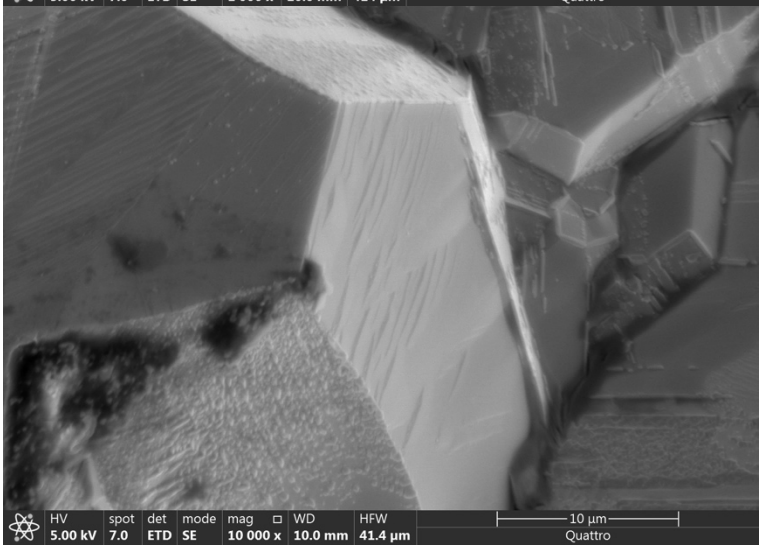

Figure 19 SEM images of penetrated part of negatively charged ceramic coated at 25% of limiting current. (a) 250X. (b) 1000X. (c) 10,000X. Please refer to Fig.11(a) for the electrochemical method to obtain this sample

a

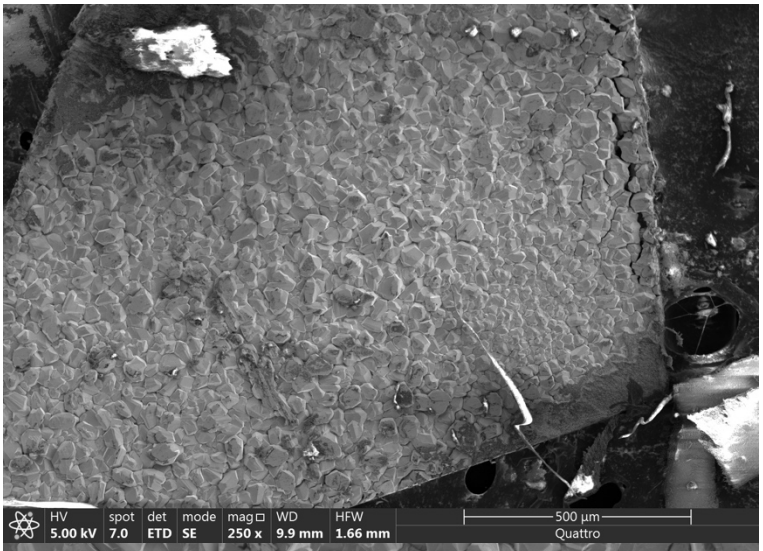

b

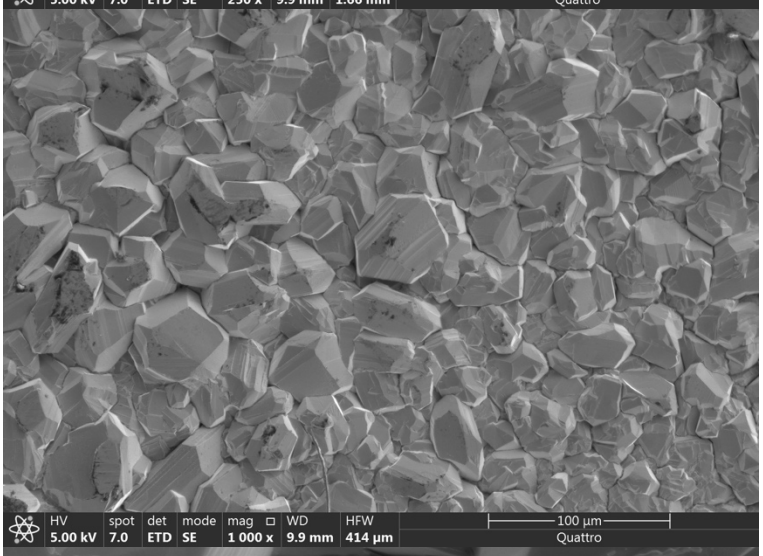

c

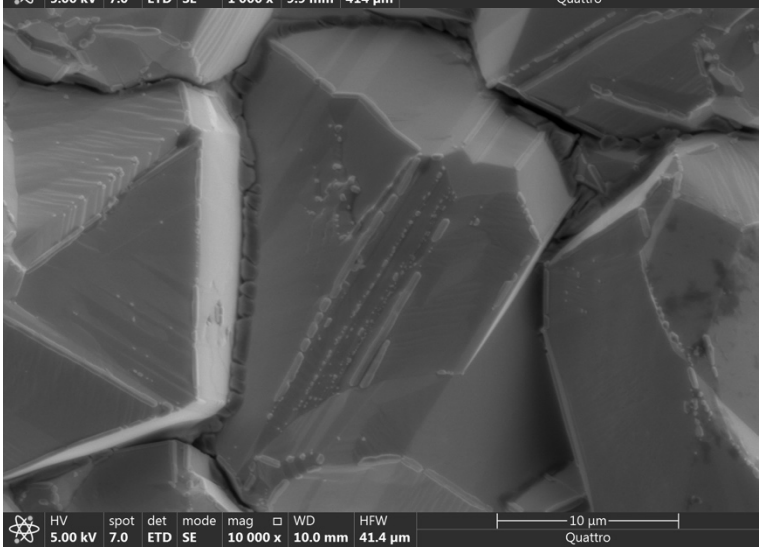

Figure 20 SEM images of penetrated part of negatively charged ceramic coated at 50% of limiting current. (a) 250X. (b) 1000X. (c) 10,000X. Please refer to Fig.12(a) for the electrochemical method to obtain this sample

a

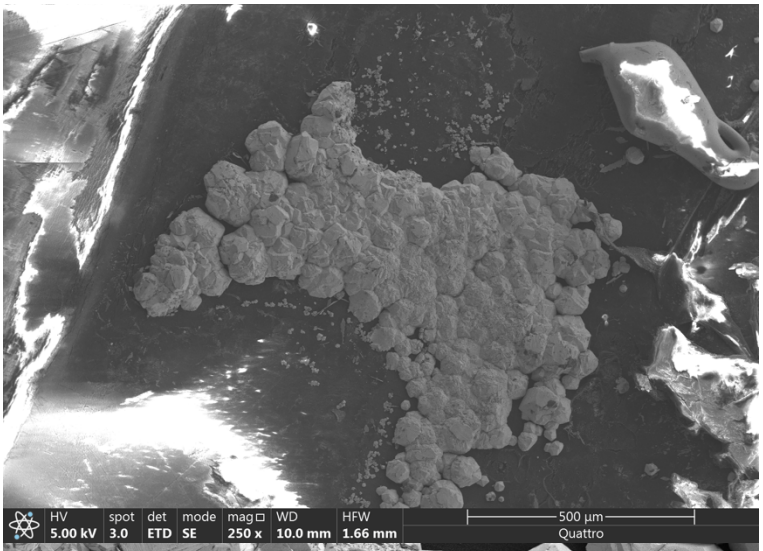

b

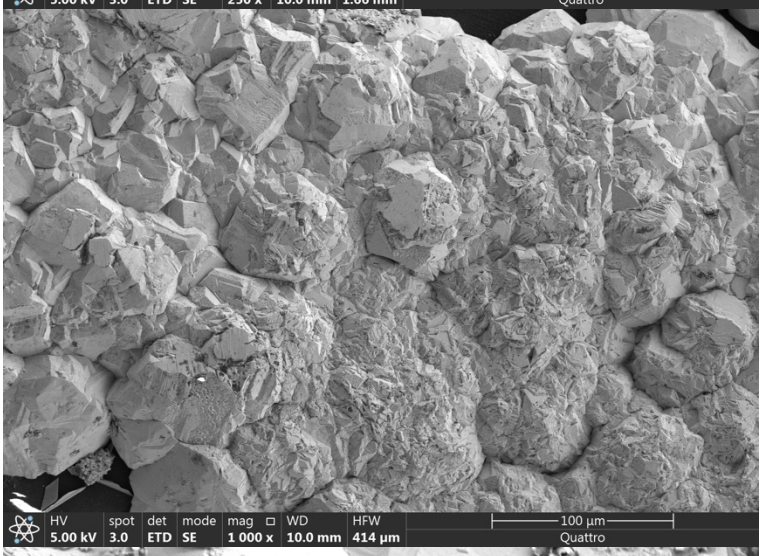

c

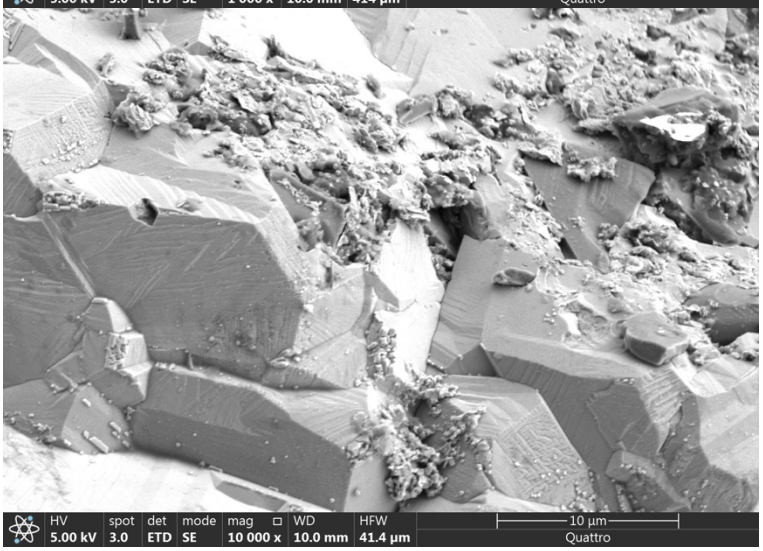

Figure 21 SEM images of unpenetrated part of negatively charged tri-layer PE at 10% of limiting current. (a) 250X. (b) 1000X. (c) 10,000X. Please refer to Fig.10(b) for the electrochemical method to obtain this sample

a

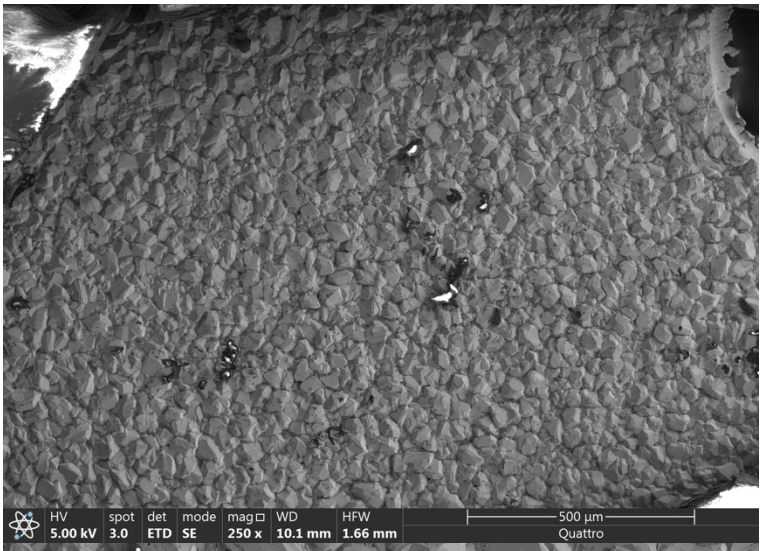

b

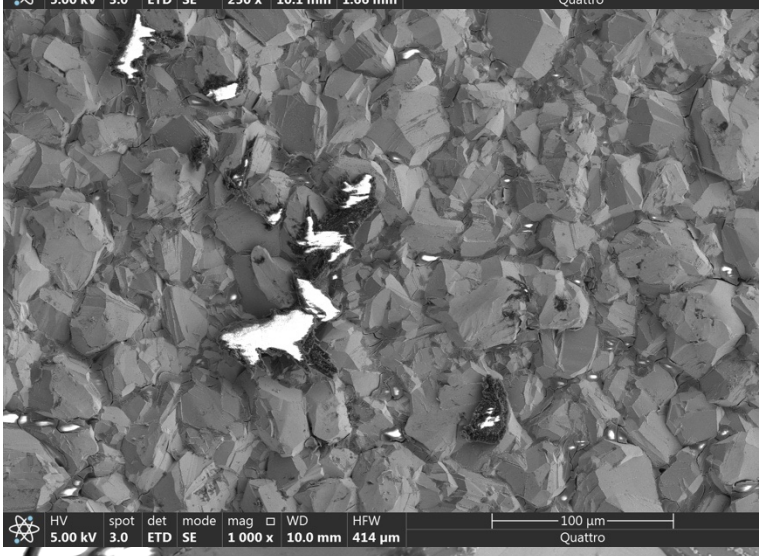

c

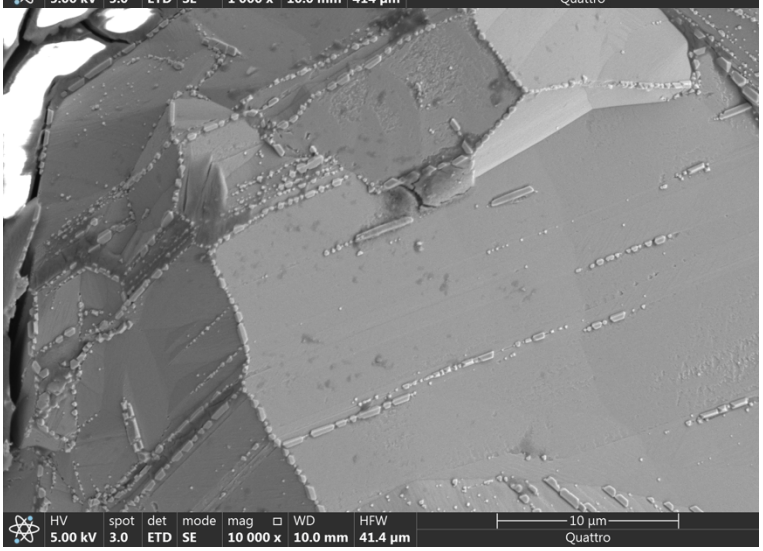

Figure 22 SEM images of unpenetrated part of negatively charged tri-layer PE at 25% of limiting current. (a) 250X. (b) 1000X. (c) 10,000X. Please refer to Fig.11(b) for the electrochemical method to obtain this sample

a

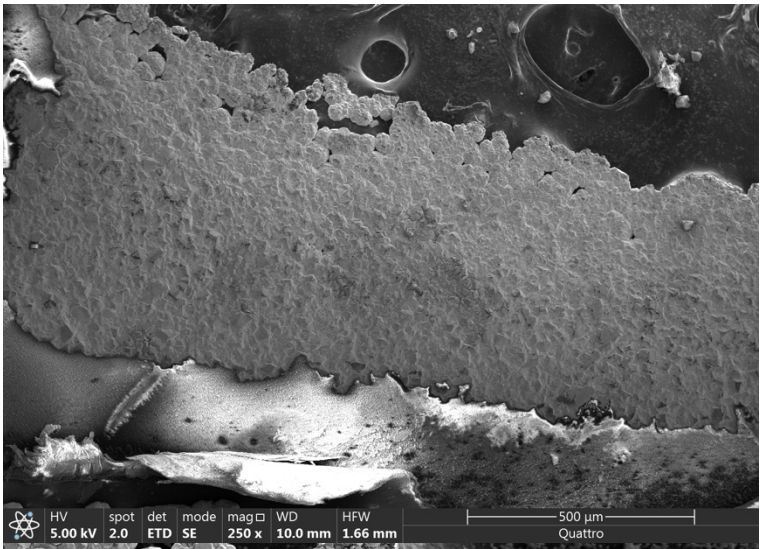

b

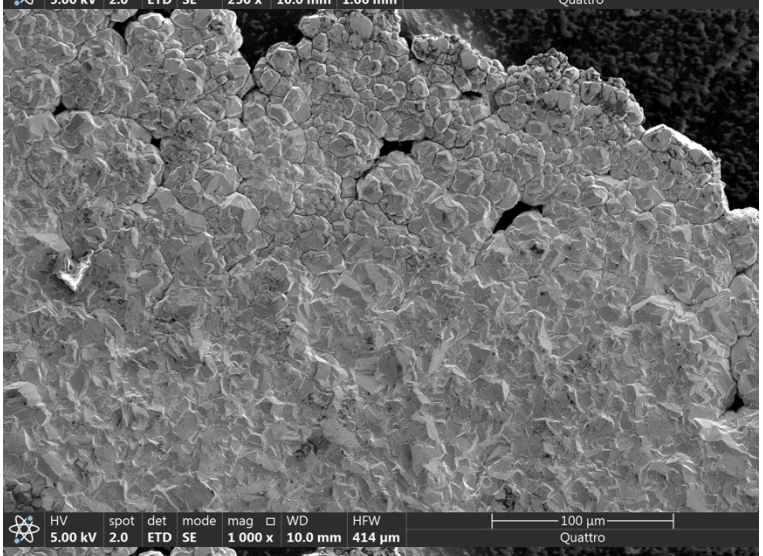

c

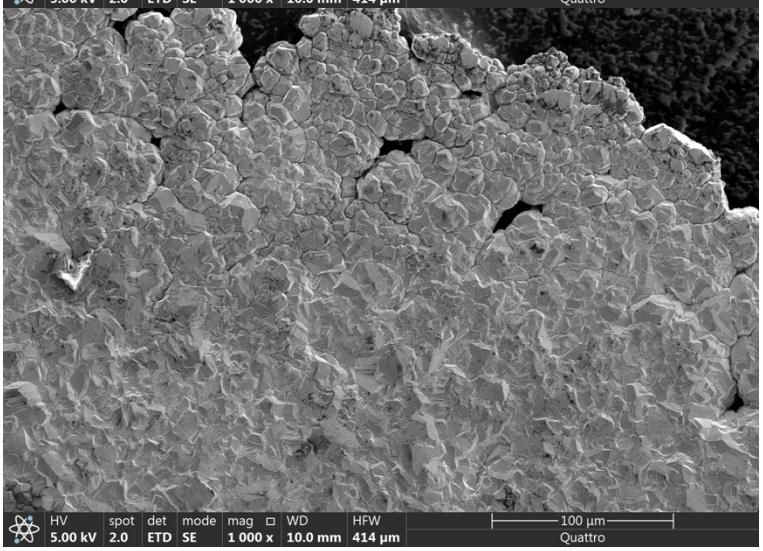

Figure 23 SEM images of unpenetrated part of negatively charged tri-layer PE at 50% of limiting current. (a) 250X. (b) 1000X. (c) 10,000X. Please refer to Fig.12(b) for the electrochemical method to obtain this sample

a

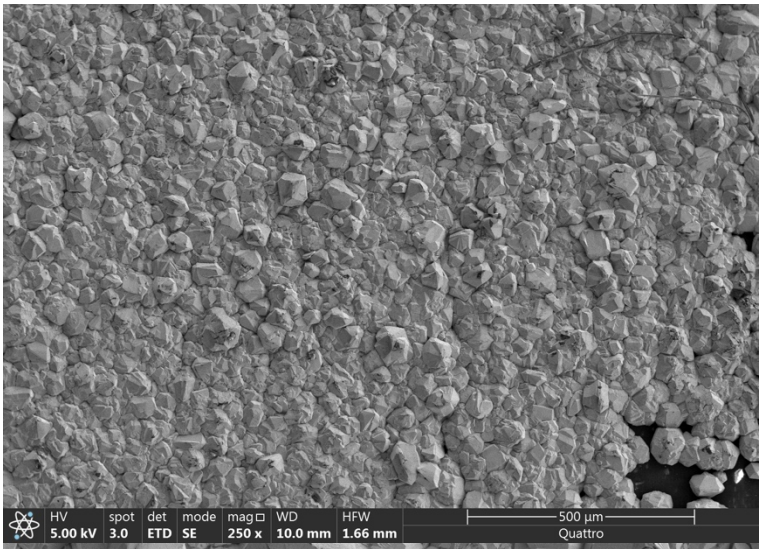

b

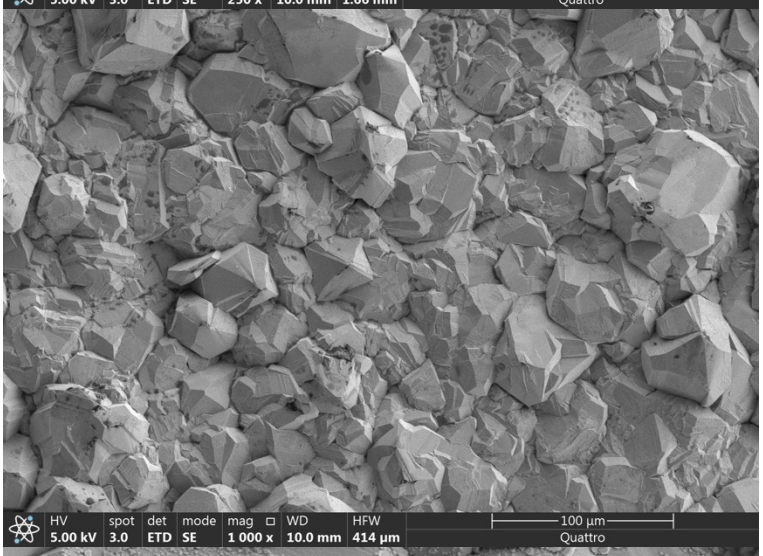

c

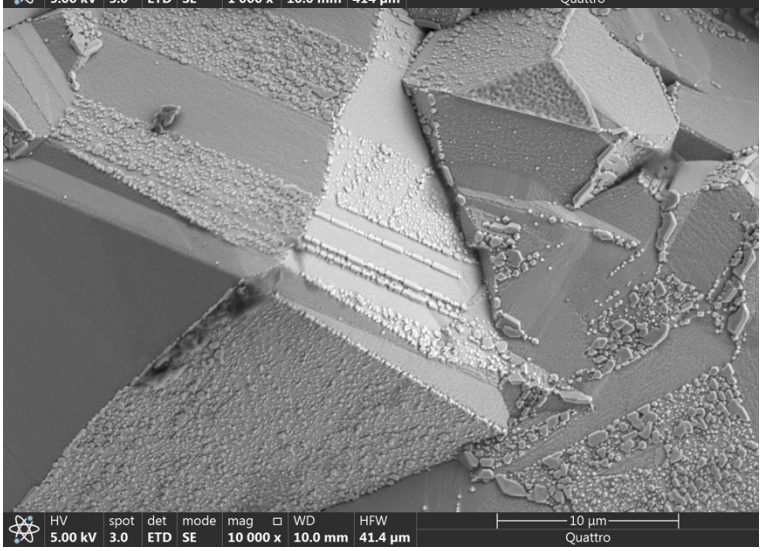

Figure 24 SEM images of penetrated part of negatively charged tri-layer PE at 10% of limiting current. (a) 250X. (b) 1000X. (c) 10,000X. Please refer to Fig.10(b) for the electrochemical method to obtain this sample

a

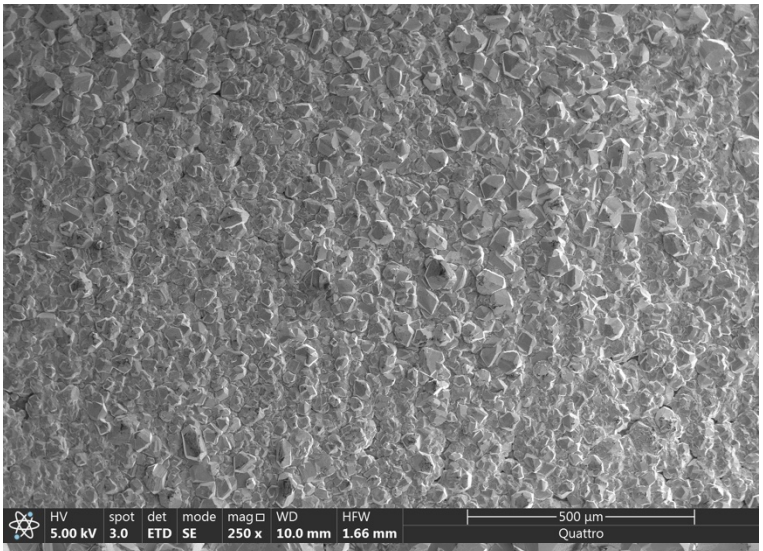

b

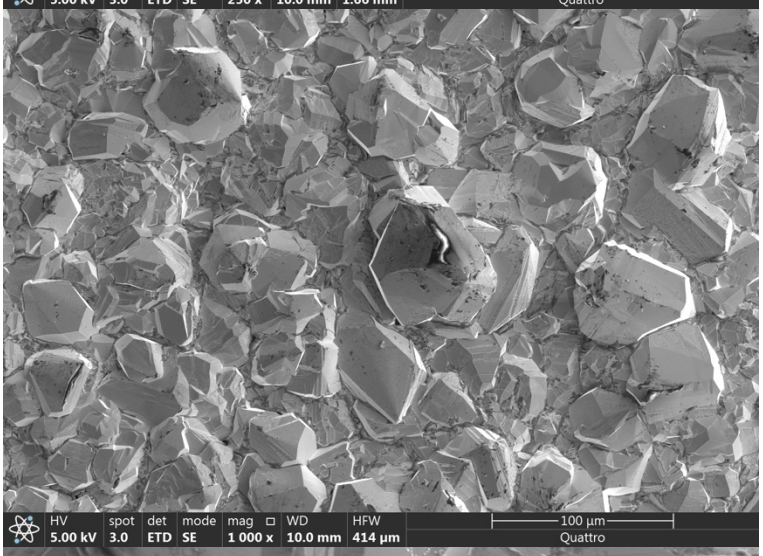

c

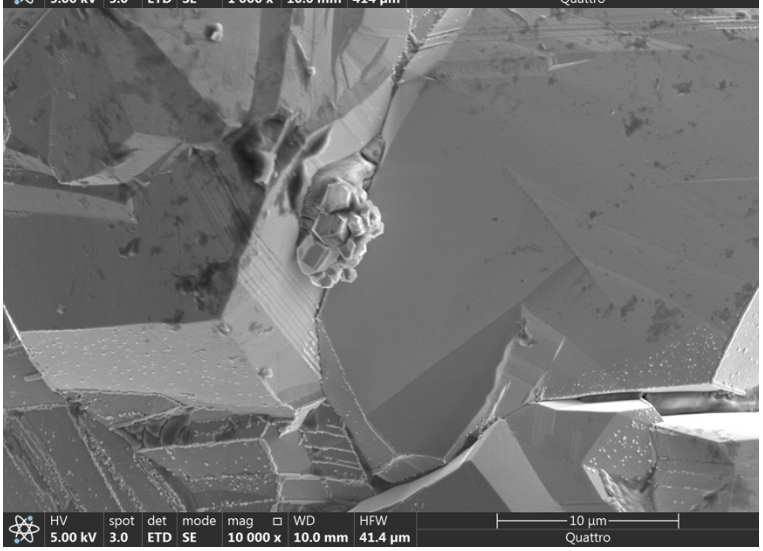

Figure 25 SEM images of penetrated part of negatively charged tri-layer PE at 25% of limiting current. (a) 250X. (b) 1000X. (c) 10,000X. Please refer to Fig.11(b) for the electrochemical method to obtain this sample

a

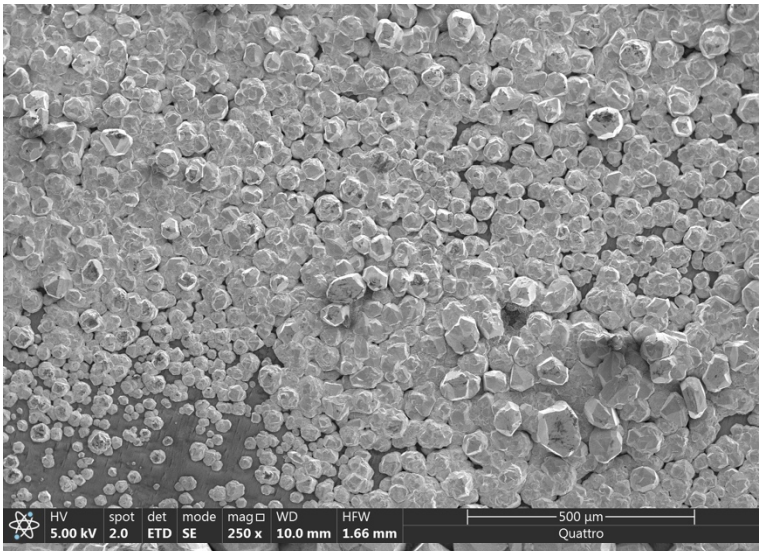

b

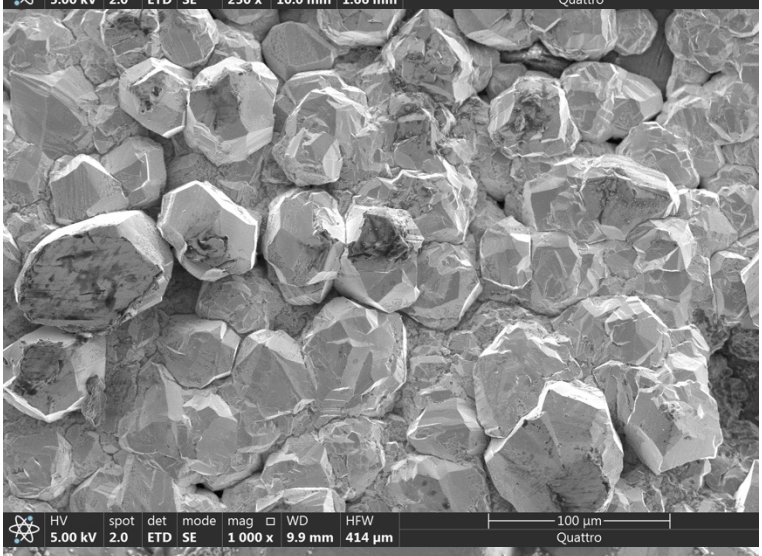

c

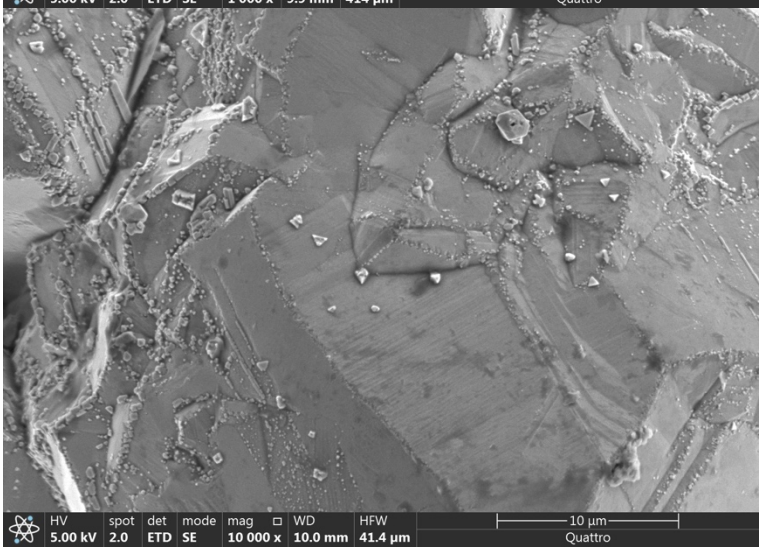

Figure 26 SEM images of penetrated part of negatively charged tri-layer PE at 50% of limiting current. (a) 250X. (b) 1000X. (c) 10,000X. Please refer to Fig.12(b) for the electrochemical method to obtain this sample

a

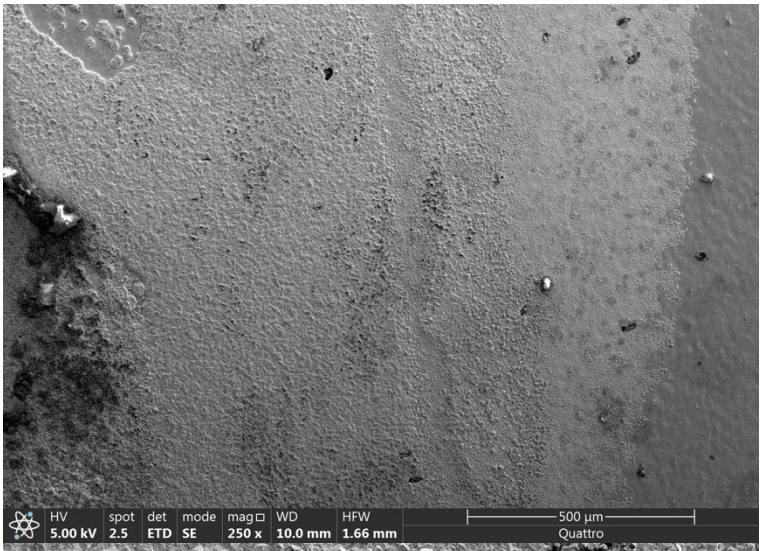

b

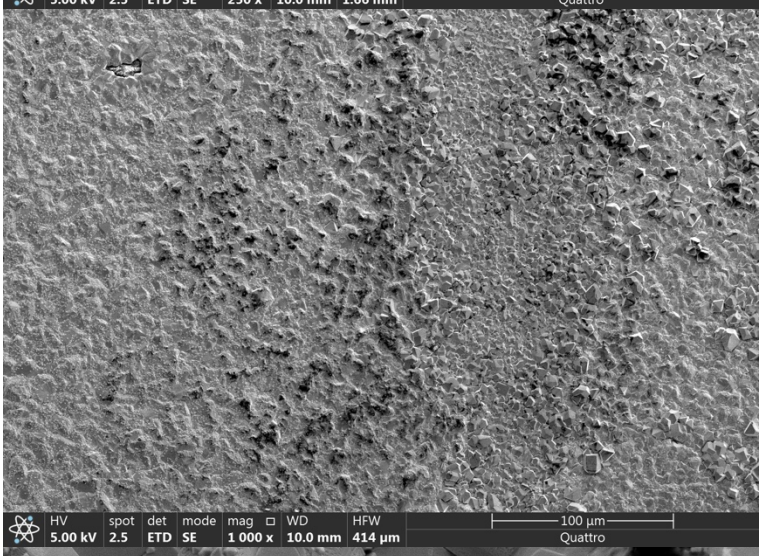

c

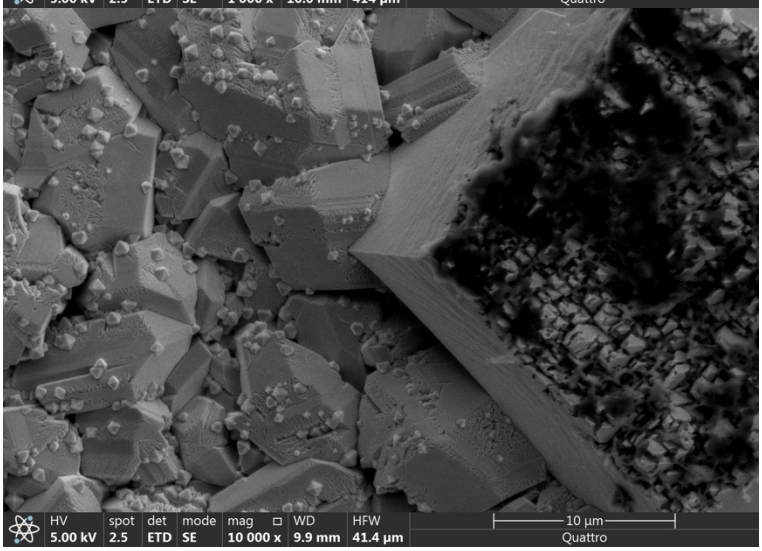

Figure 27 SEM images of unpenetrated part of negatively charged cellulose nitrate at 10% of limiting current. (a) 250X. (b) 1000X. (c) 10,000X. Please refer to Fig.10(c) for the electrochemical method to obtain this sample

a

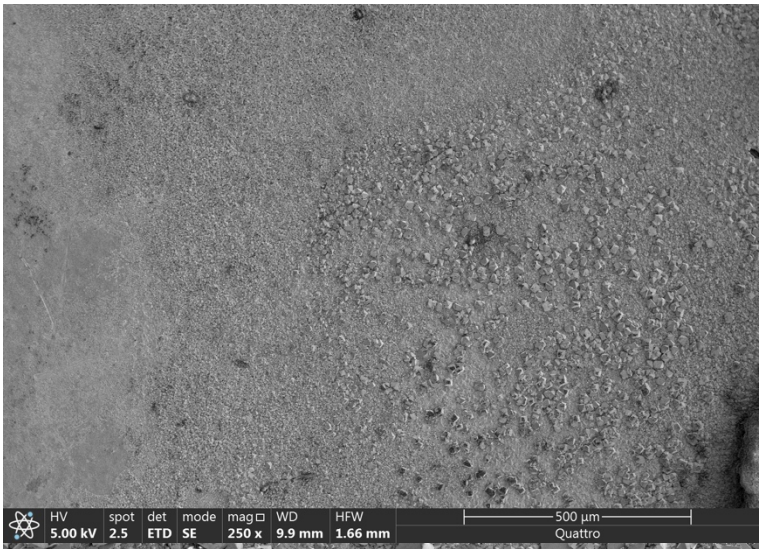

b

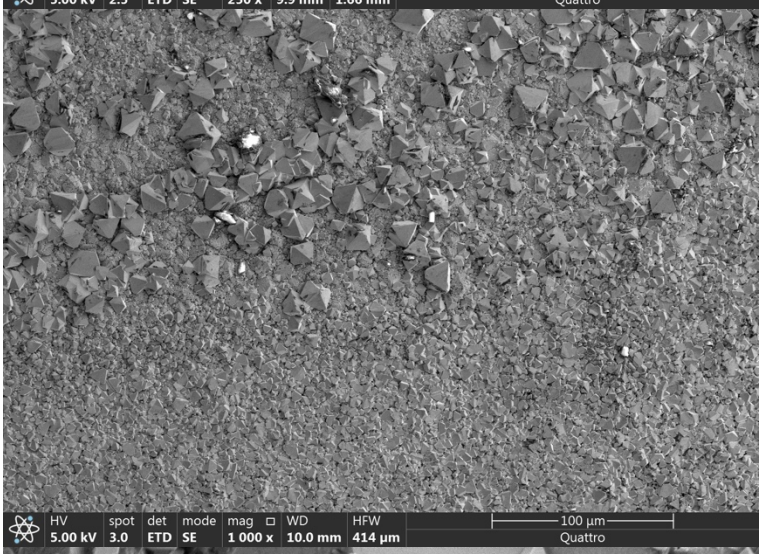

c

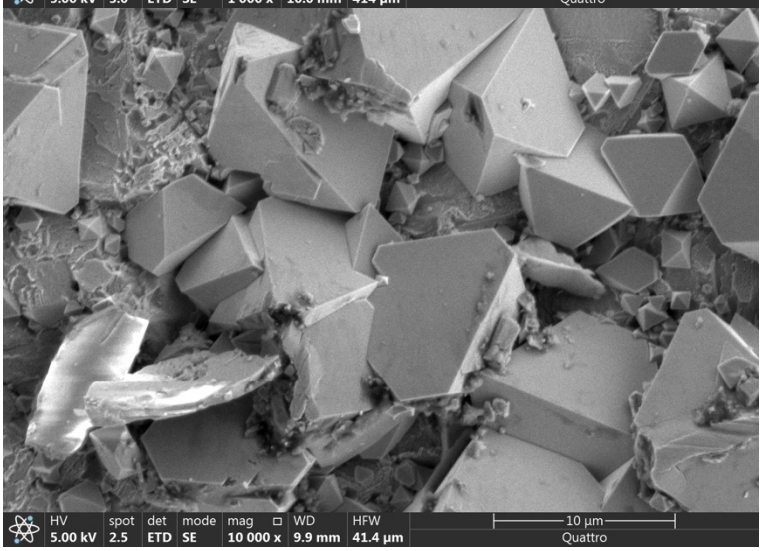

Figure 28 SEM images of unpenetrated part of negatively charged cellulose nitrate at 25% of limiting current. (a) 250X. (b) 1000X. (c) 10,000X. Please refer to Fig.11(c) for the electrochemical method to obtain this sample

a

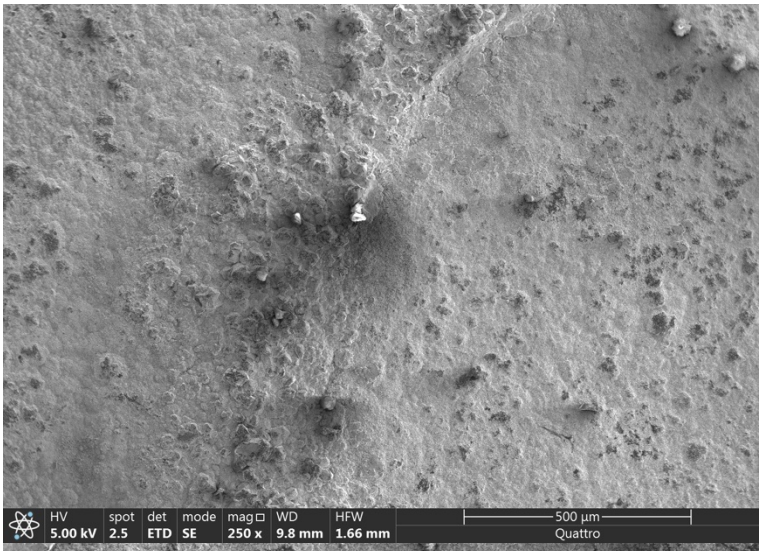

b

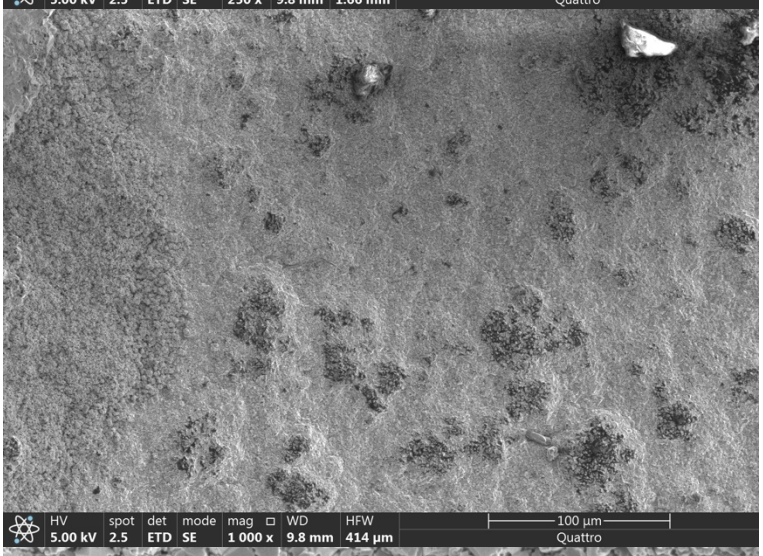

c

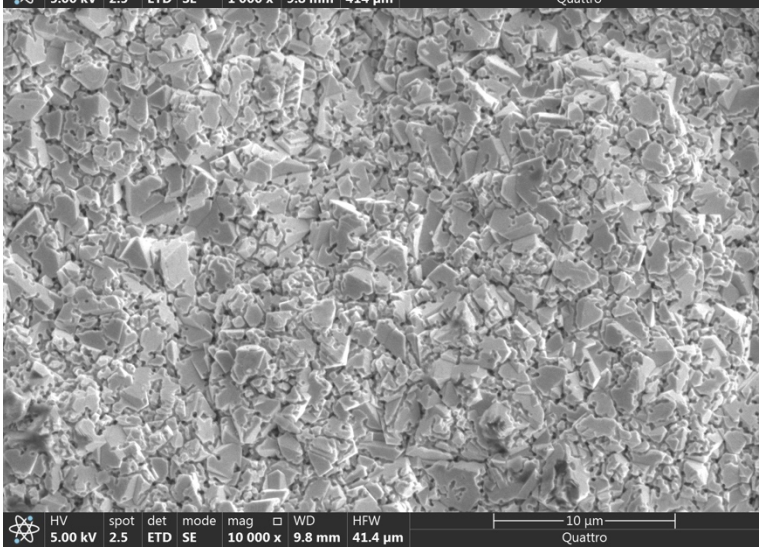

Figure 29 SEM images of unpenetrated part of negatively charged cellulose nitrate at 50% of limiting current. (a) 250X. (b) 1000X. (c) 10,000X. Please refer to Fig.12(c) for the electrochemical method to obtain this sample

a

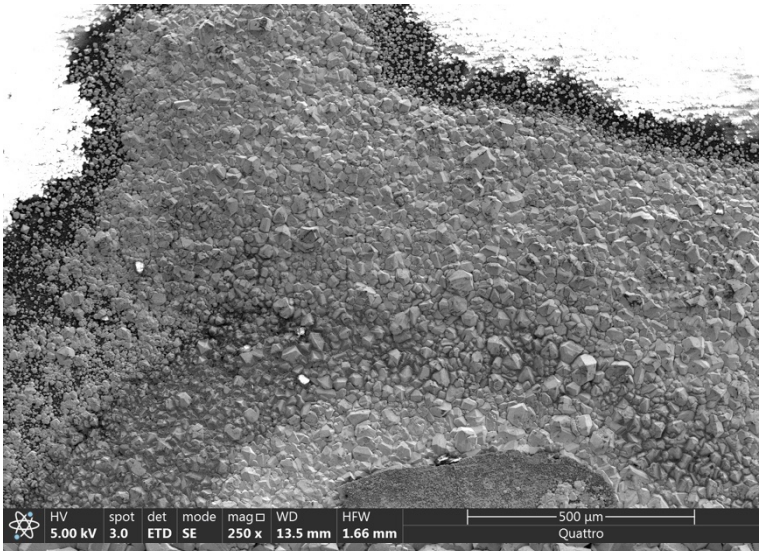

b

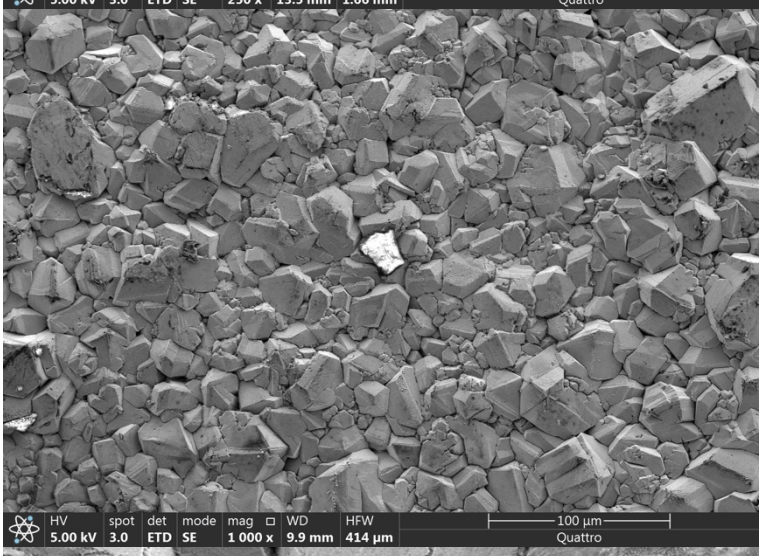

c

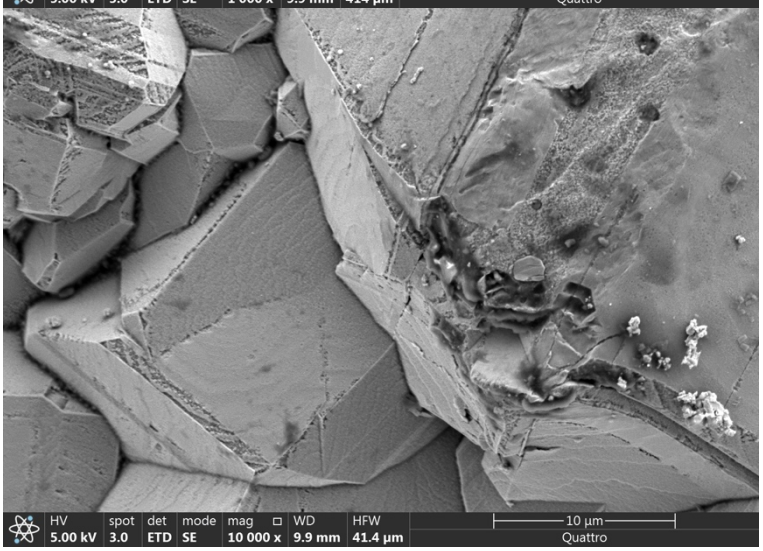

Figure 30 SEM images of penetrated part of negatively charged cellulose nitrate at 10% of limiting current. (a) 250X. (b) 1000X. (c) 10,000X. Please refer to Fig.10(c) for the electrochemical method to obtain this sample

a

b

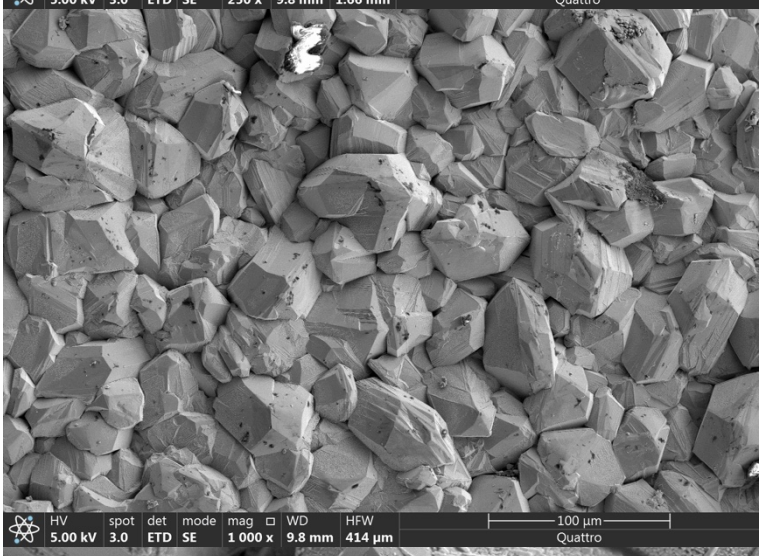

c

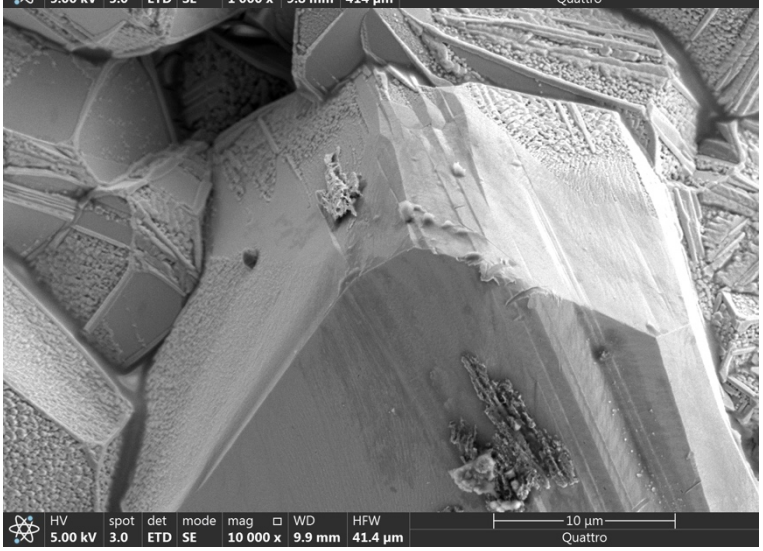

Figure 31 SEM images of penetrated part of negatively charged cellulose nitrate at 25% of limiting current. (a) 250X. (b) 1000X. (c) 10,000X. Please refer to Fig.11(c) for the electrochemical method to obtain this sample

a

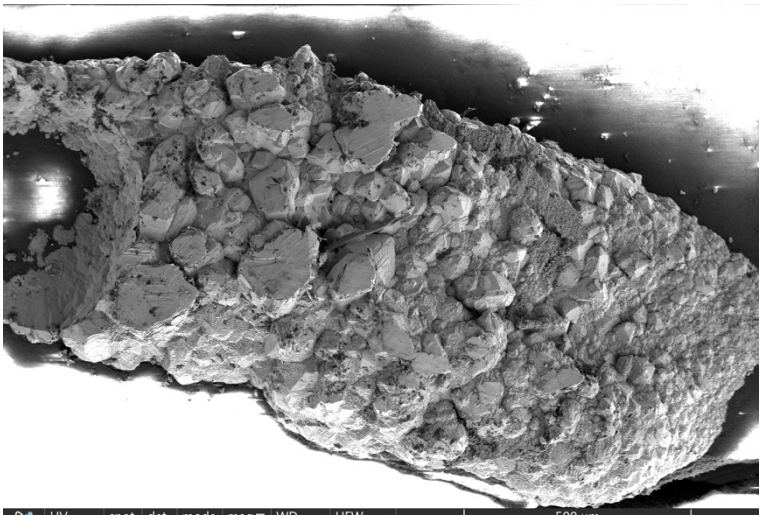

b

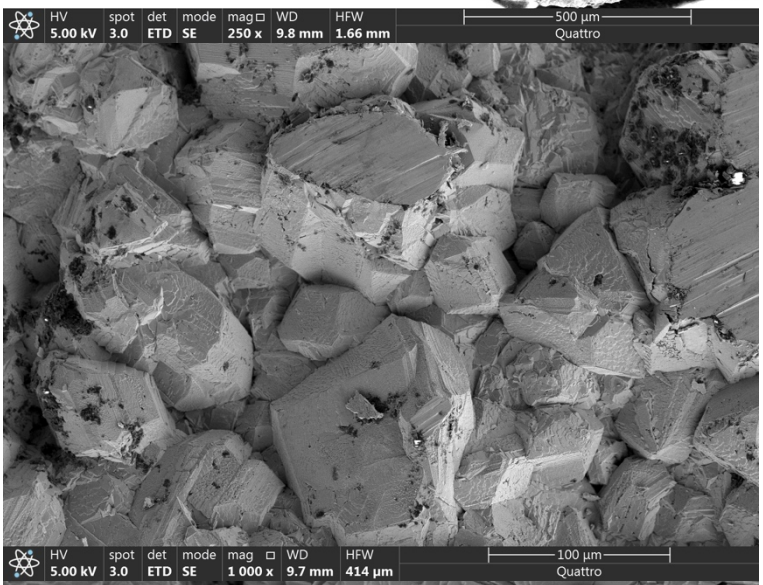

c

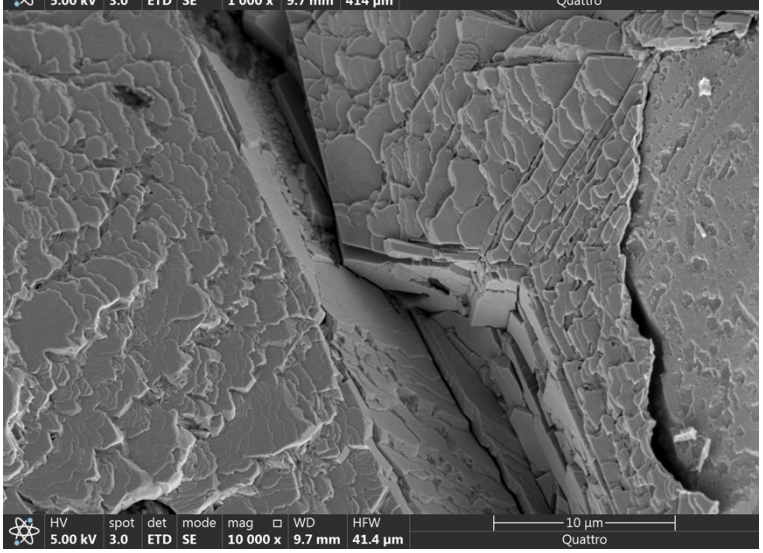

Figure 32 SEM images of penetrated part of negatively charged cellulose nitrate at 50% of limiting current. (a) 250X. (b) 1000X. (c) 10,000X. Please refer to Fig.12(c) for the electrochemical method to obtain this sample

a

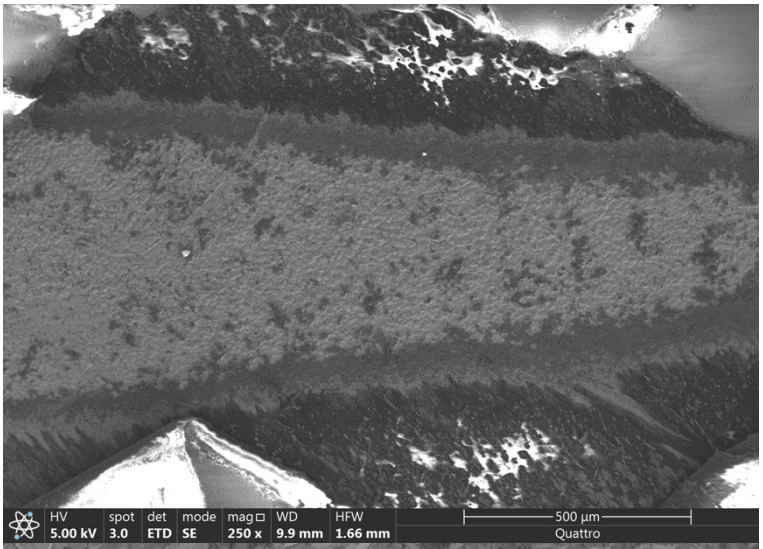

b

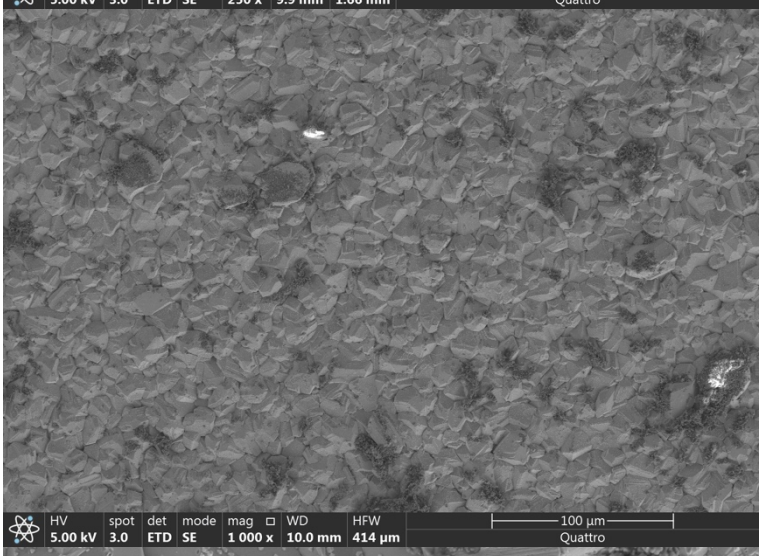

c

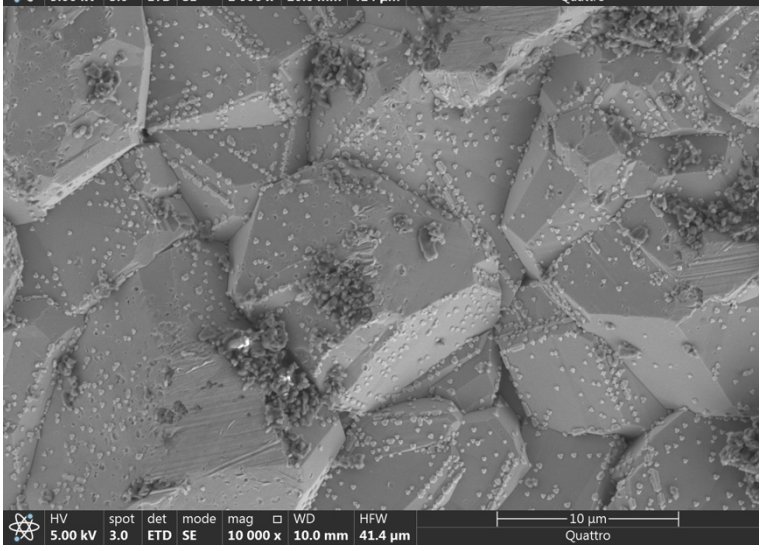

Figure 32 SEM images of unpenetrated part of positively charged ceramic coated at 10% of limiting current. (a) 250X. (b) 1000X. (c) 10,000X. Please refer to Fig.10(a) for the electrochemical method to obtain this sample

a

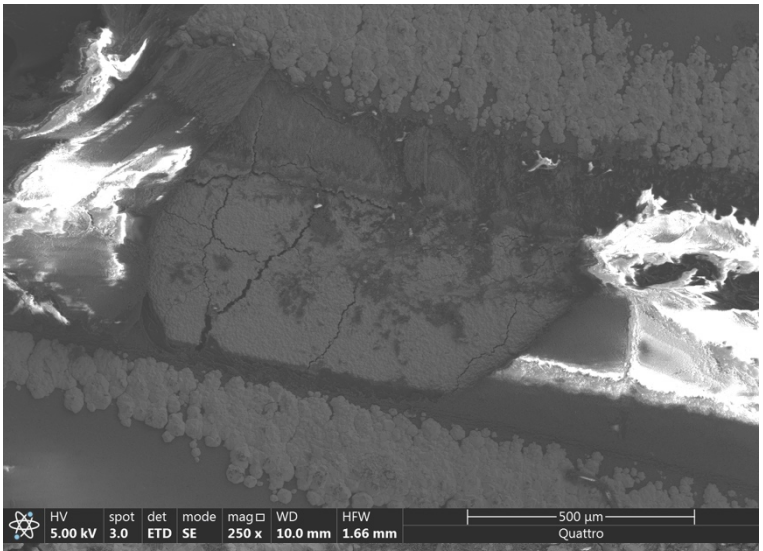

b

c

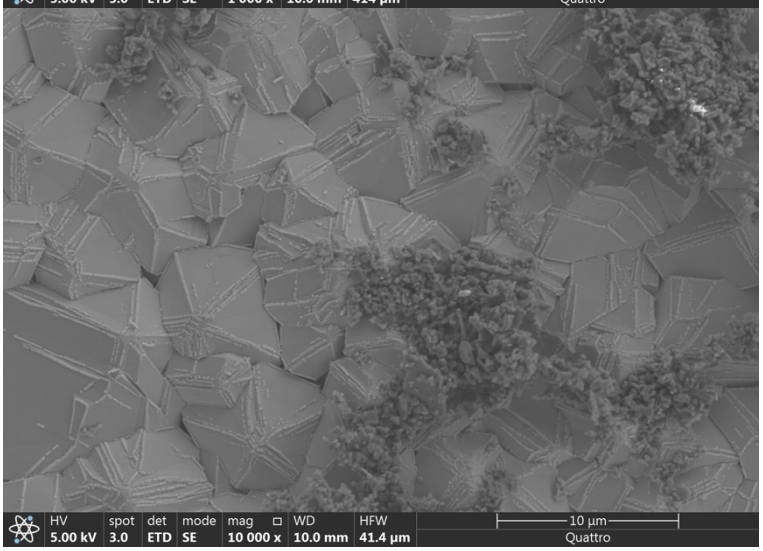

Figure 34 SEM images of unpenetrated part of positively charged ceramic coated at 25% of limiting current. (a) 250X. (b) 1000X. (c) 10,000X. Please refer to Fig.11(a) for the electrochemical method to obtain this sample

a

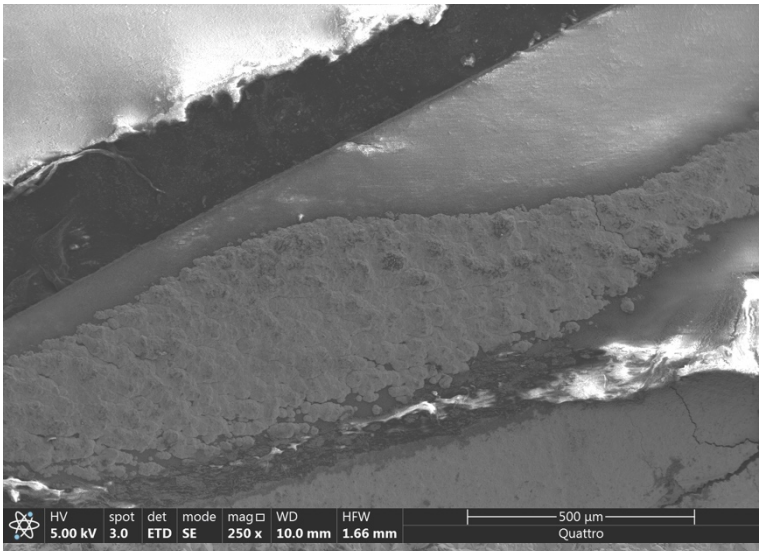

b

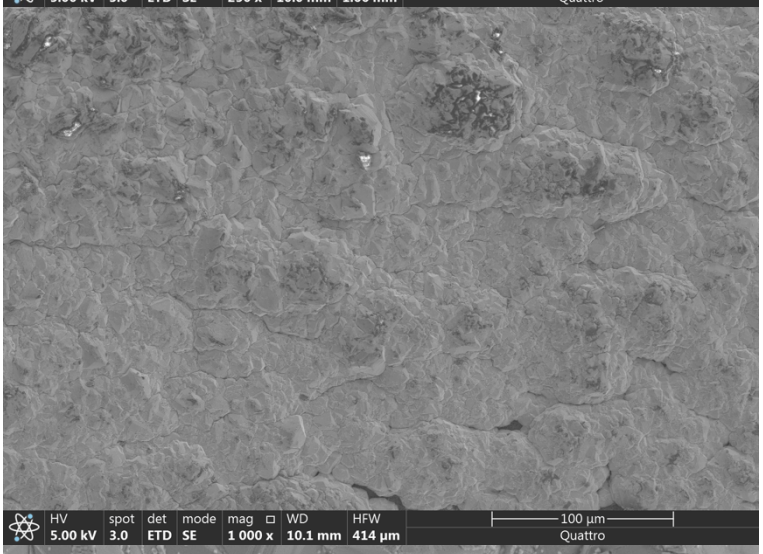

c

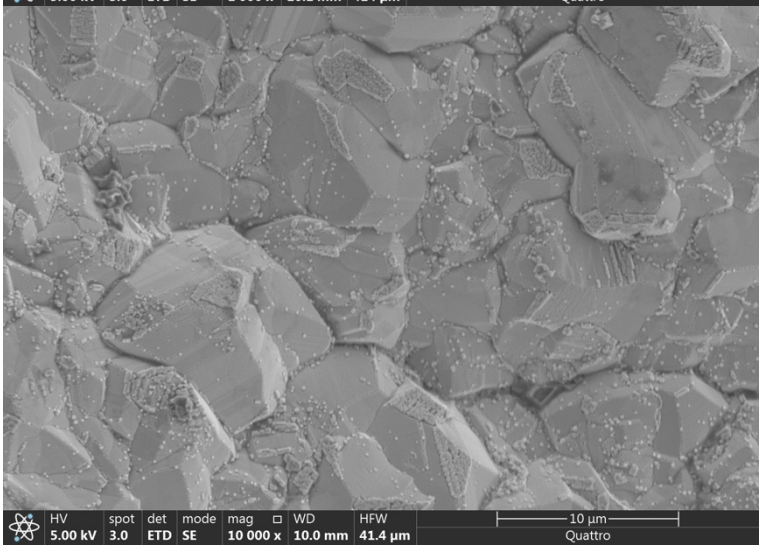

Figure 35 SEM images of unpenetrated part of positively charged ceramic coated at 50% of limiting current. (a) 250X. (b) 1000X. (c) 10,000X. Please refer to Fig.12(a) for the electrochemical method to obtain this sample

a

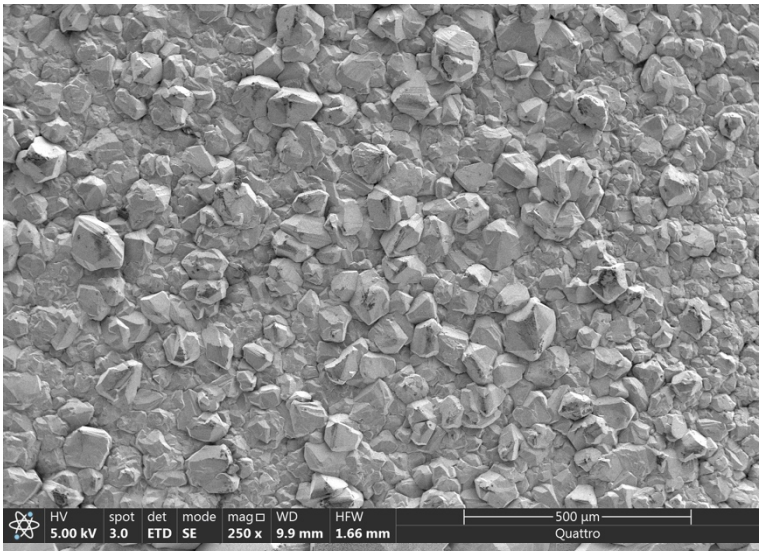

b

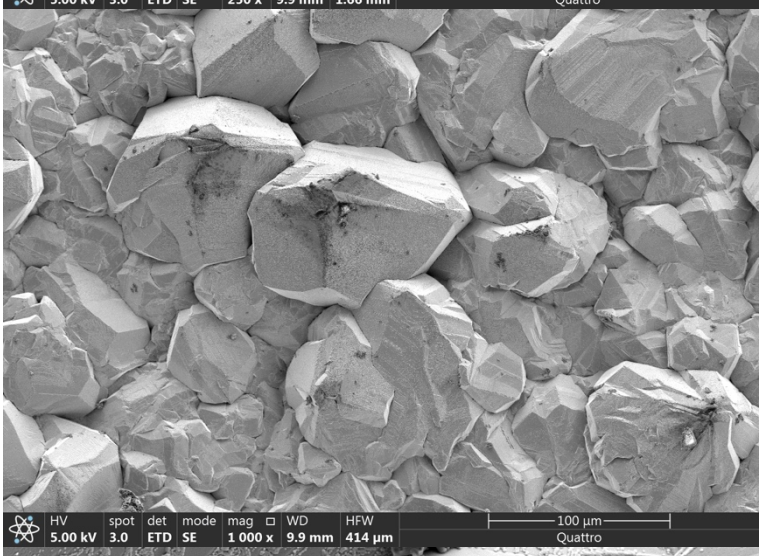

c

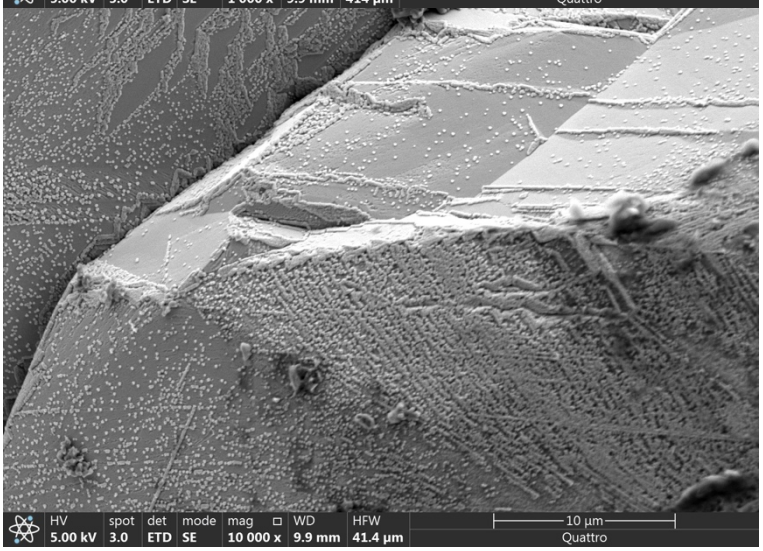

Figure 36 SEM images of penetrated part of positively charged ceramic coated at 10% of limiting current. (a) 250X. (b) 1000X. (c) 10,000X. Please refer to Fig.10(a) for the electrochemical method to obtain this sample

a

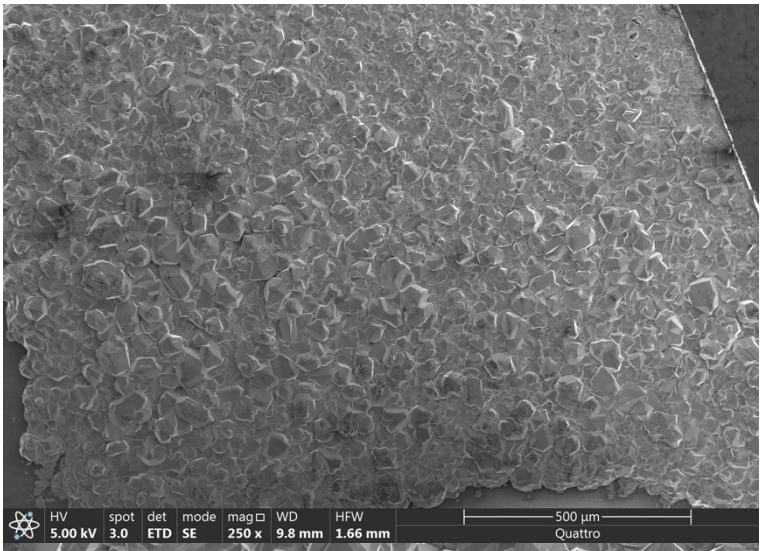

b

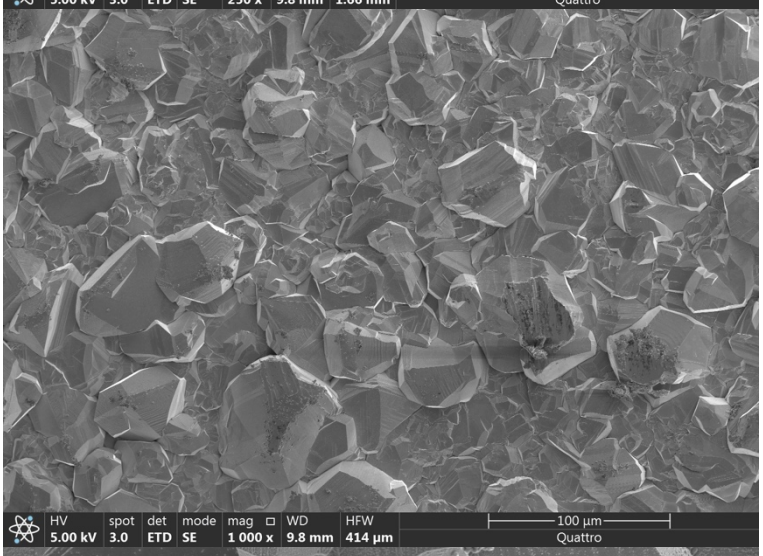

c

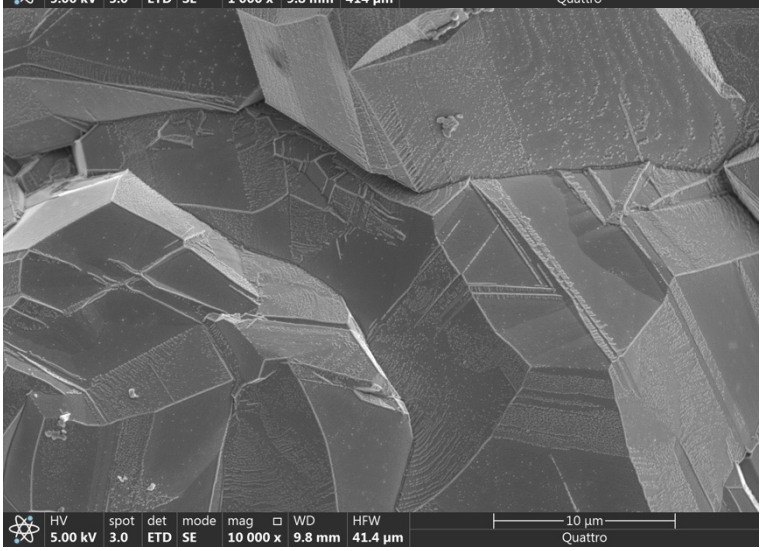

Figure 37 SEM images of penetrated part of positively charged ceramic coated at 25% of limiting current. (a) 250X. (b) 1000X. (c) 10,000X. Please refer to Fig.11(a) for the electrochemical method to obtain this sample

a

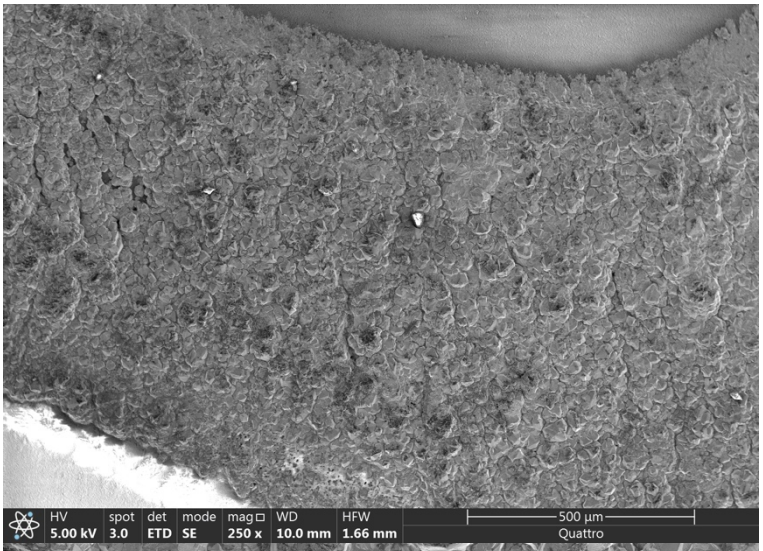

b

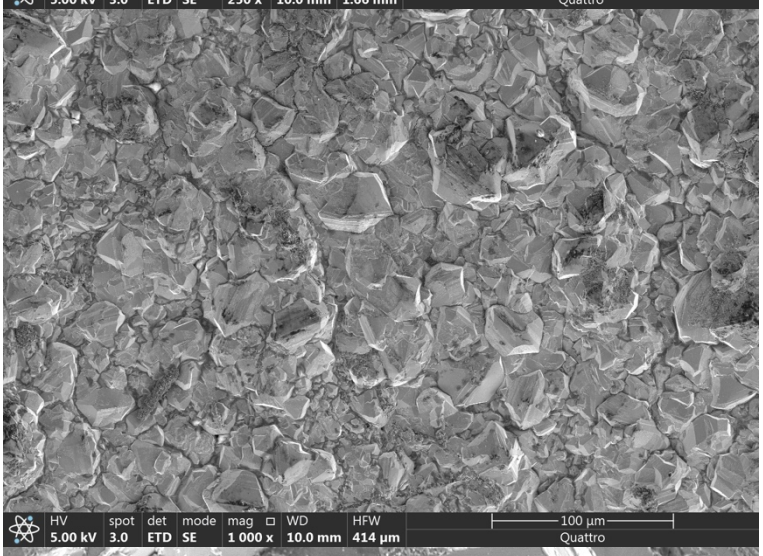

c

Figure 38 SEM images of penetrated part of positively charged ceramic coated at 50% of limiting current. (a) 250X. (b) 1000X. (c) 10,000X. Please refer to Fig.12(a) for the electrochemical method to obtain this sample

a

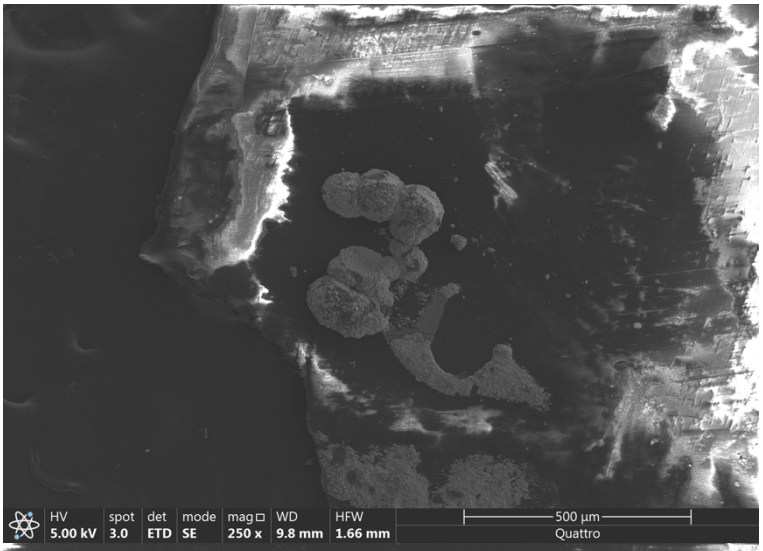

b

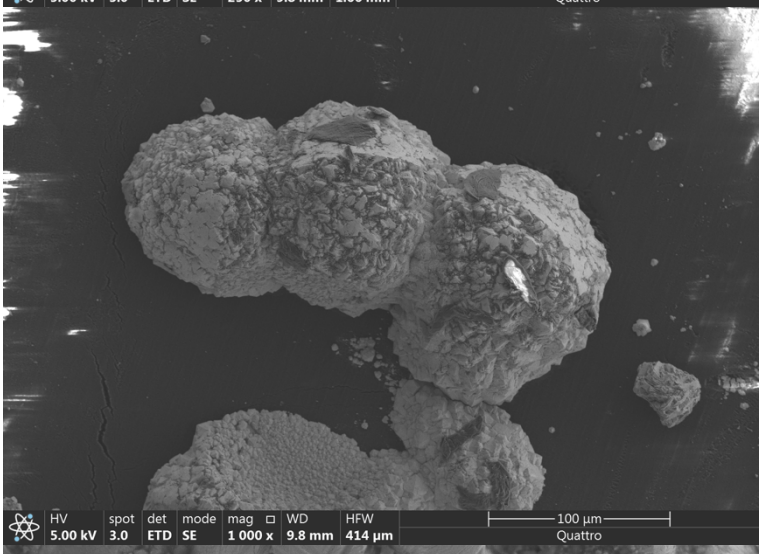

c

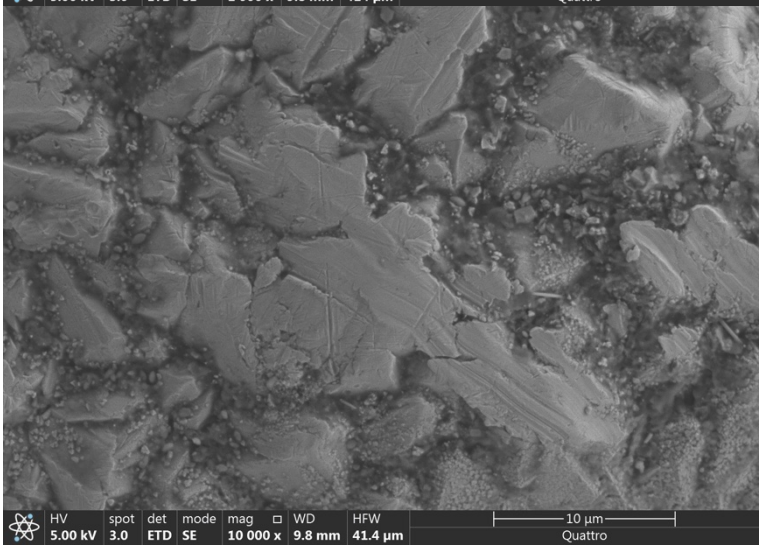

Figure 39 SEM images of unpenetrated part of positively tri-layer PE coated at 10% of limiting current. (a) 250X. (b) 1000X. (c) 10,000X. Please refer to Fig.10(b) for the electrochemical method to obtain this sample

a

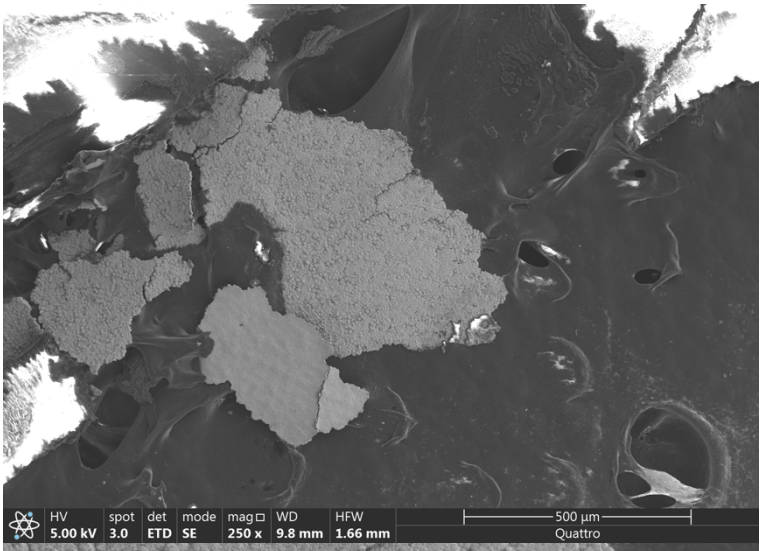

b

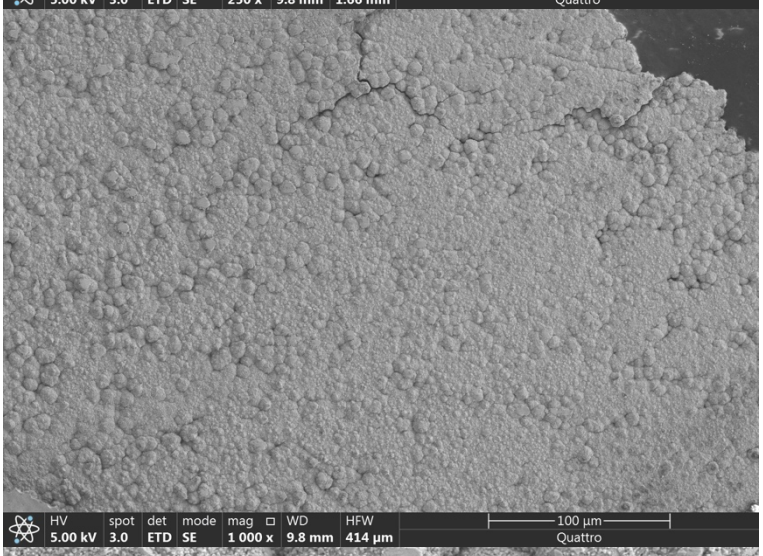

c

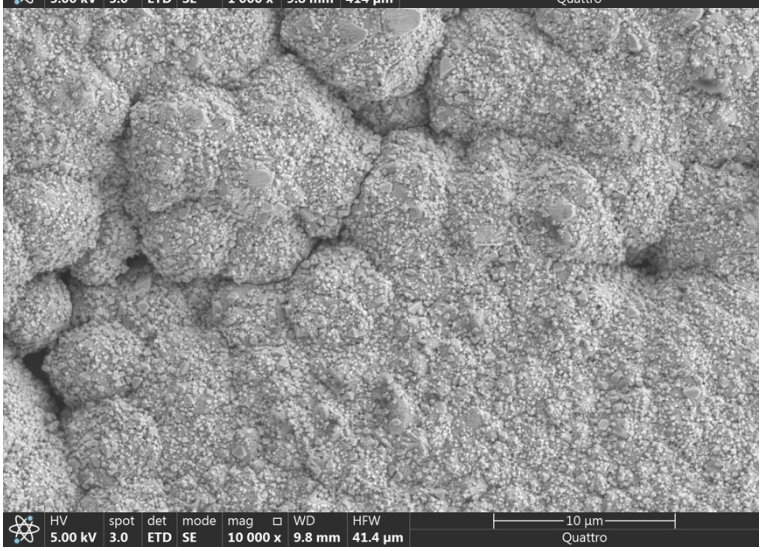

Figure 40 SEM images of unpenetrated part of positively tri-layer PE coated at 25% of limiting current. (a) 250X. (b) 1000X. (c) 10,000X. Please refer to Fig.11(b) for the electrochemical method to obtain this sample

a

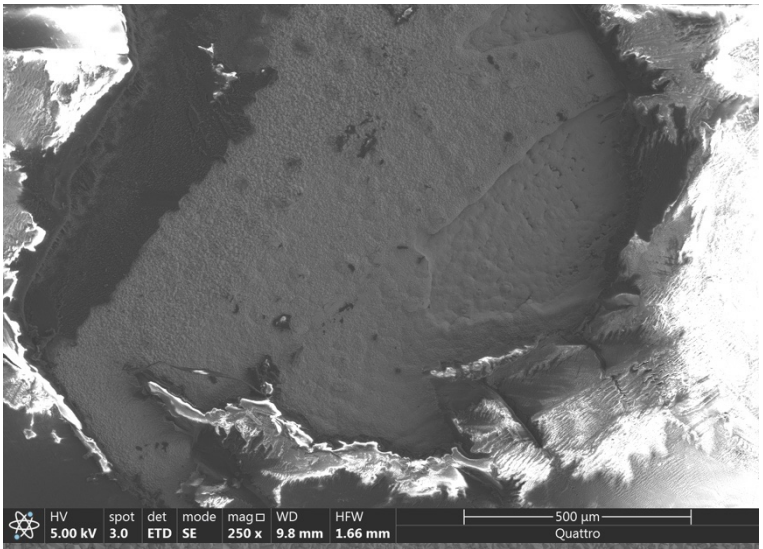

b

c

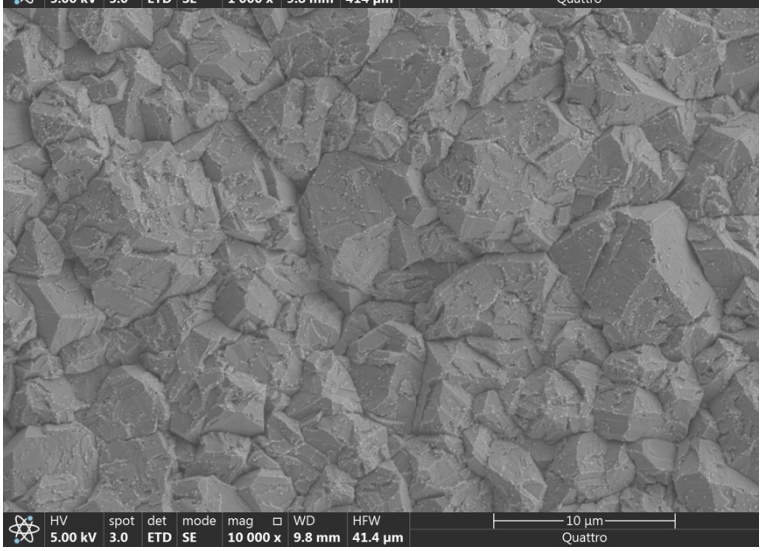

Figure 41 SEM images of unpenetrated part of positively tri-layer PE coated at 50% of limiting current. (a) 250X. (b) 1000X. (c) 10,000X. Please refer to Fig.12(b) for the electrochemical method to obtain this sample

a

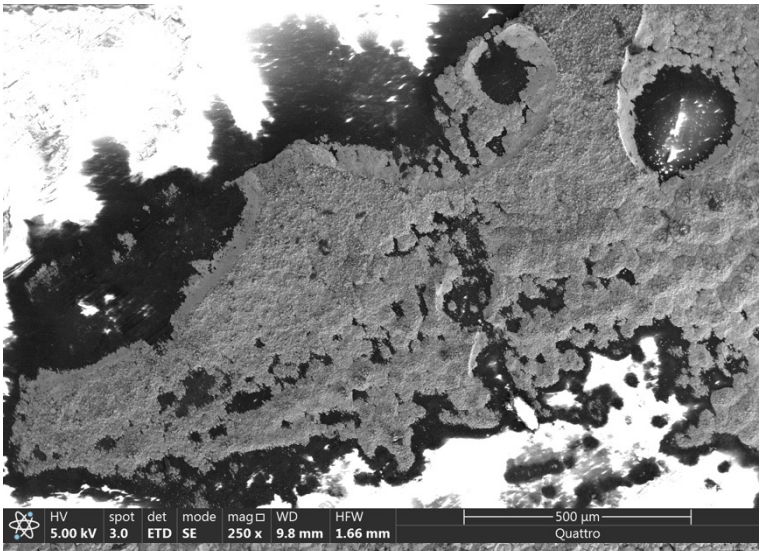

b

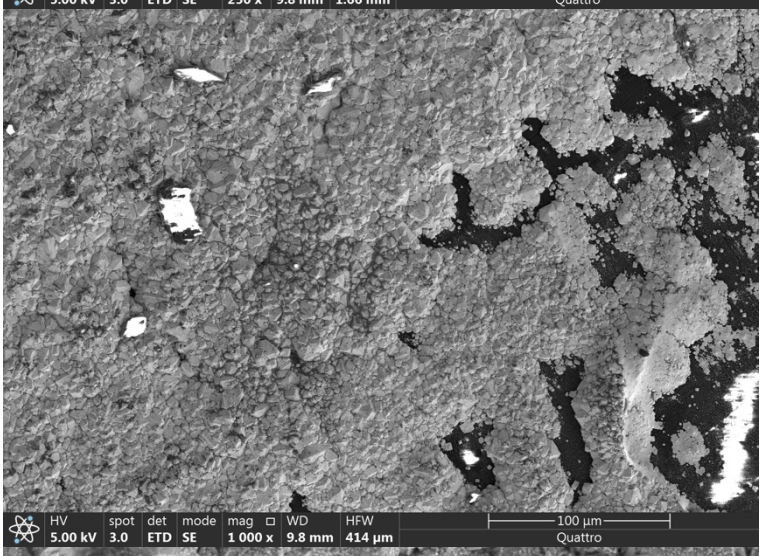

c

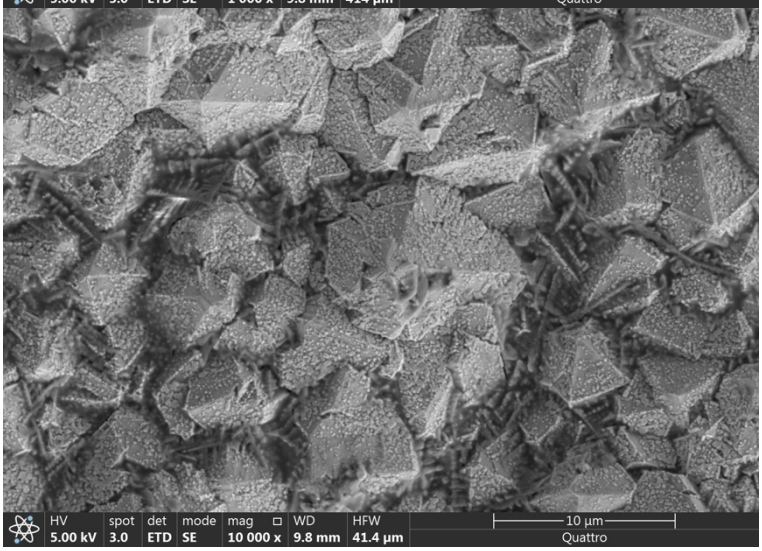

Figure 42 SEM images of penetrated part of positively tri-layer PE coated at 10% of limiting current. (a) 250X. (b) 1000X. (c) 10,000X. Please refer to Fig.10(b) for the electrochemical method to obtain this sample

a

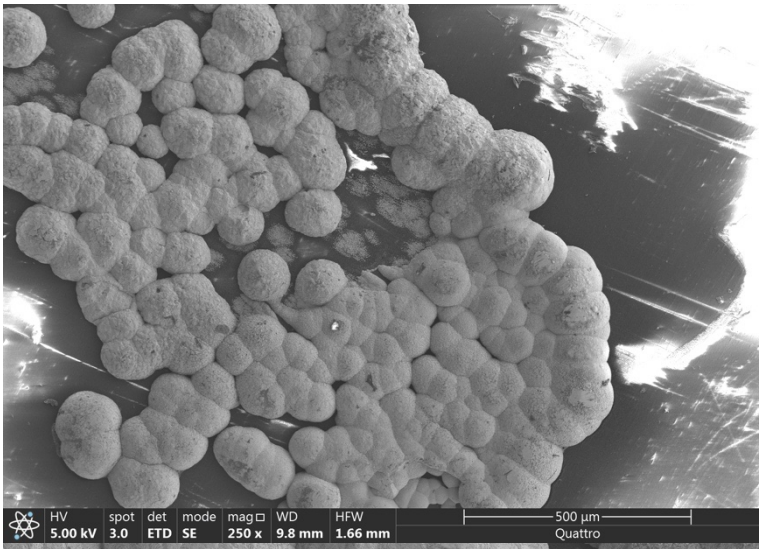

b

c

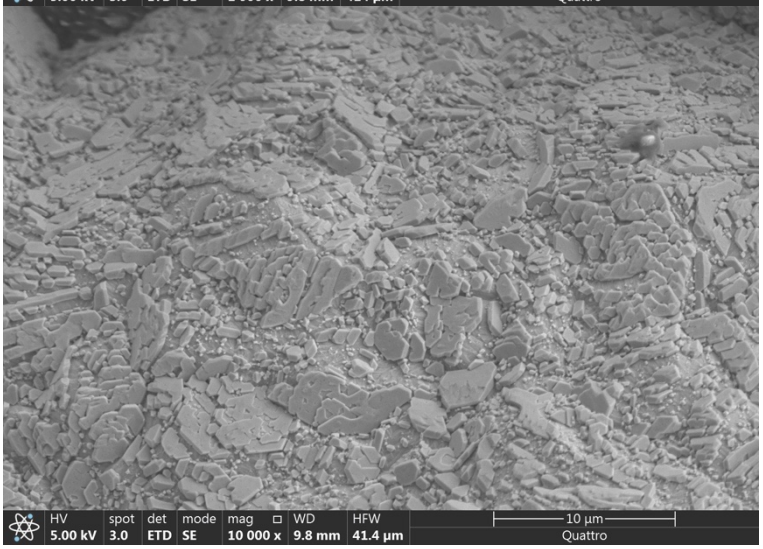

Figure 43 SEM images of penetrated part of positively tri-layer PE coated at 25% of limiting current. (a) 250X. (b) 1000X. (c) 10,000X. Please refer to Fig.11(b) for the electrochemical method to obtain this sample

a

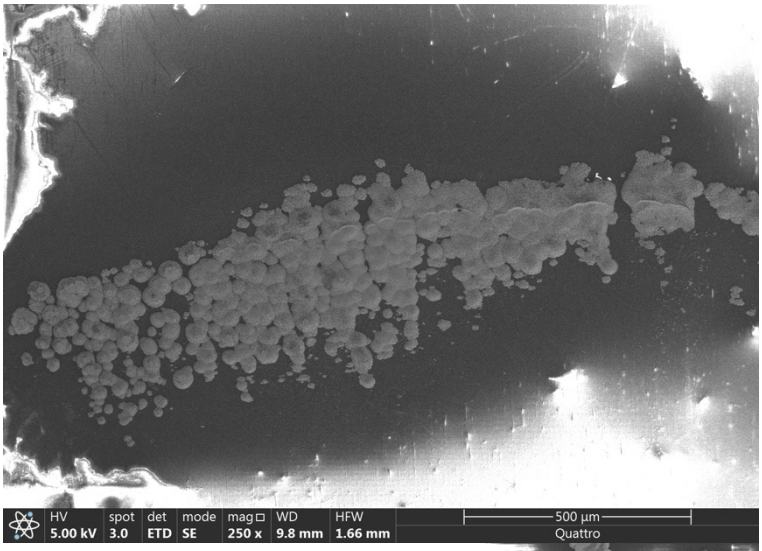

b

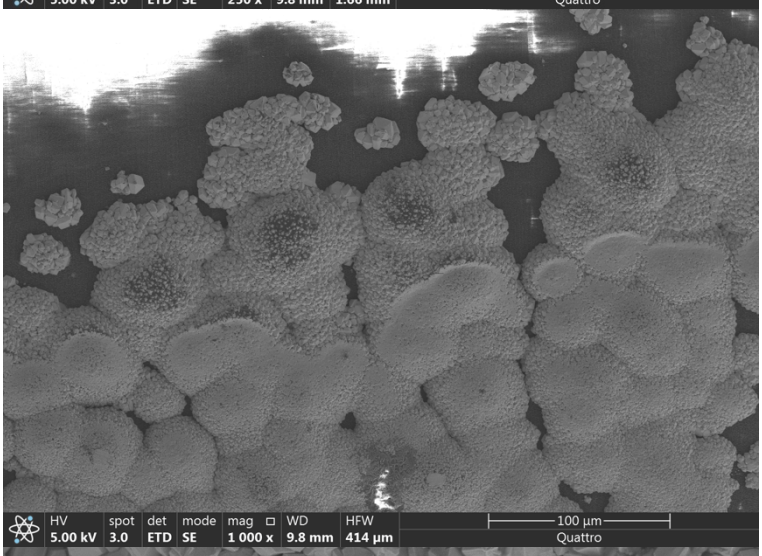

c

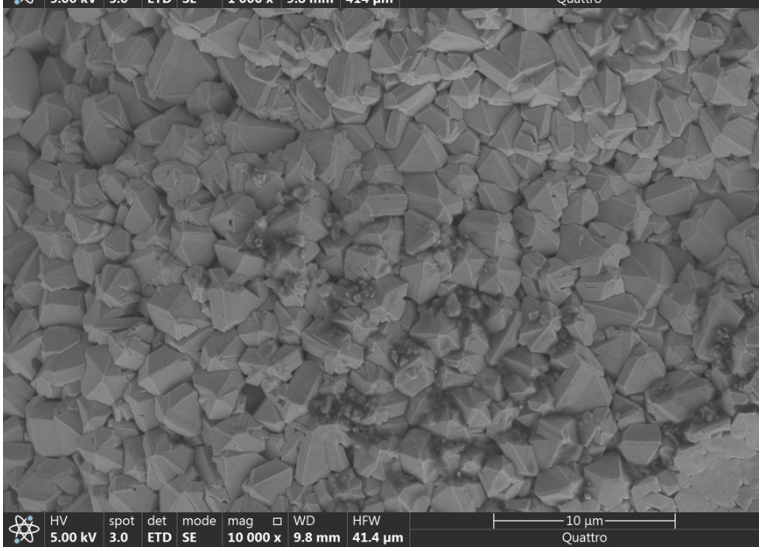

Figure 44 SEM images of penetrated part of positively tri-layer PE coated at 50% of limiting current. (a) 250X. (b) 1000X. (c) 10,000X. Please refer to Fig.12(b) for the electrochemical method to obtain this sample

a

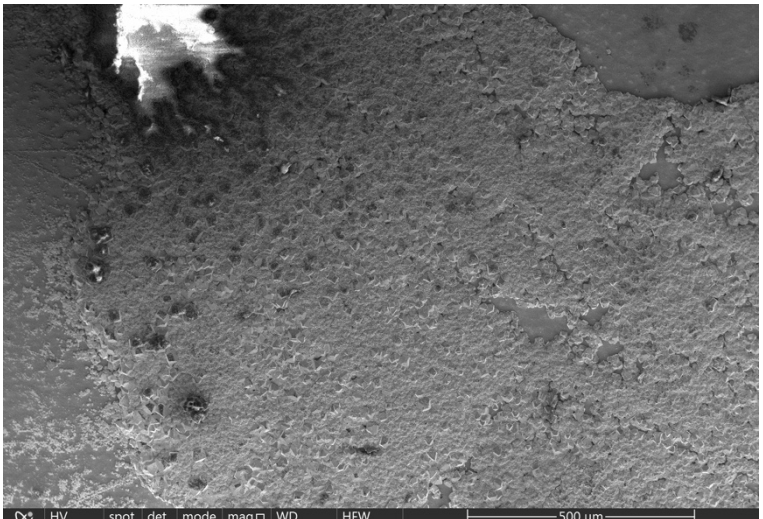

b

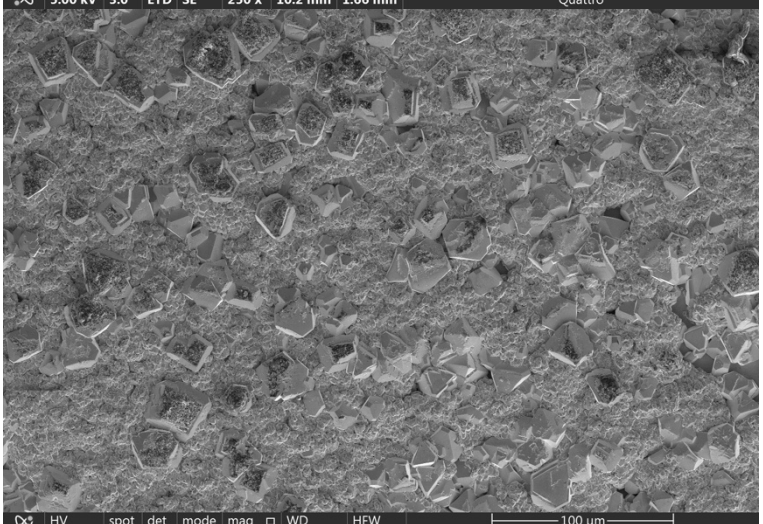

c

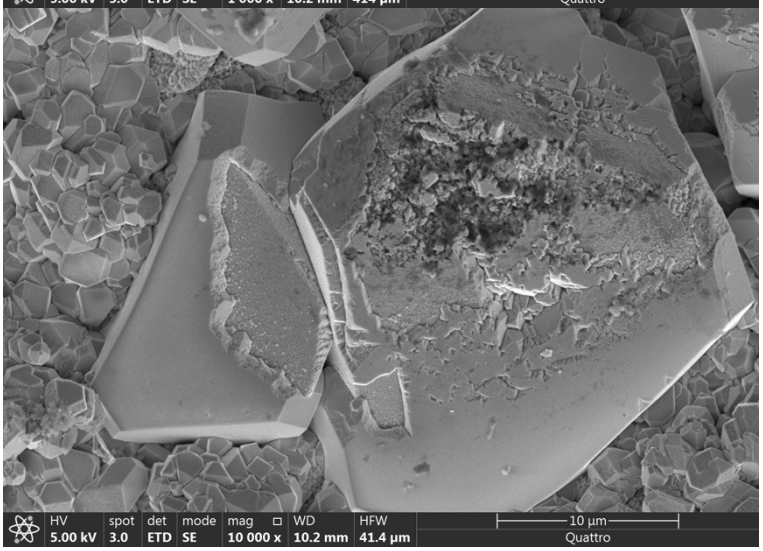

Figure 45 SEM images of unpenetrated part of positively cellulose nitrate at 10% of limiting current. (a) 250X. (b) 1000X. (c) 10,000X. Please refer to Fig.10(c) for the electrochemical method to obtain this sample

a

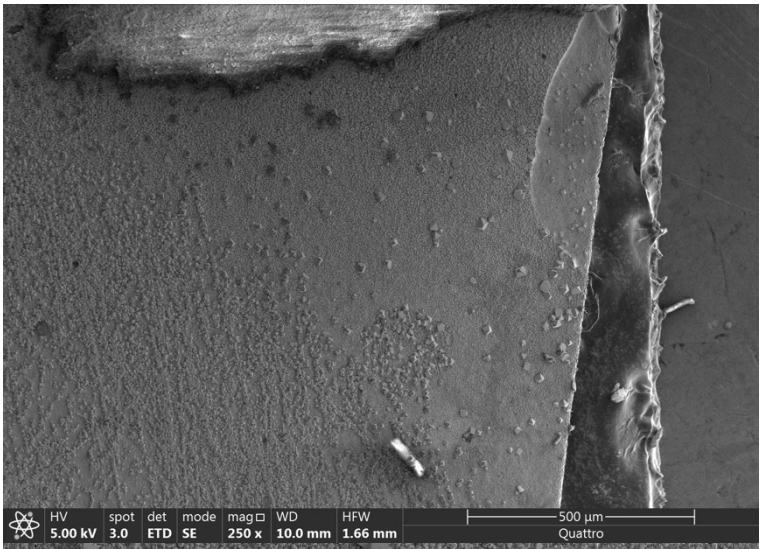

b

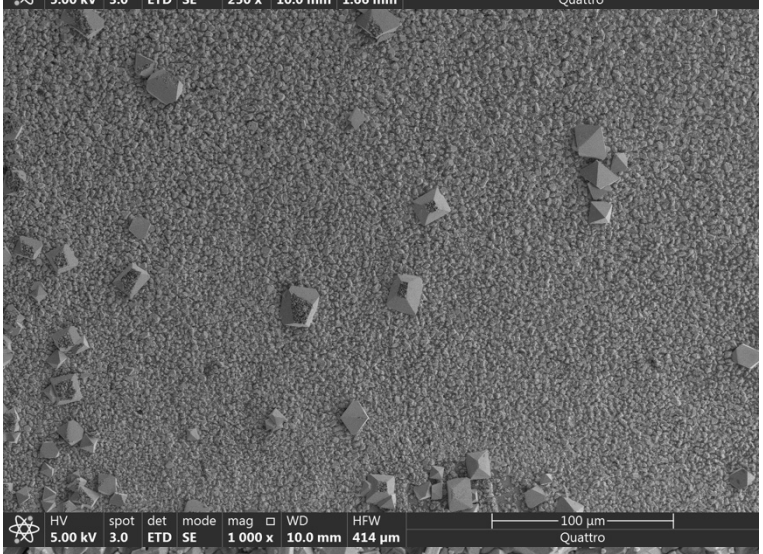

c

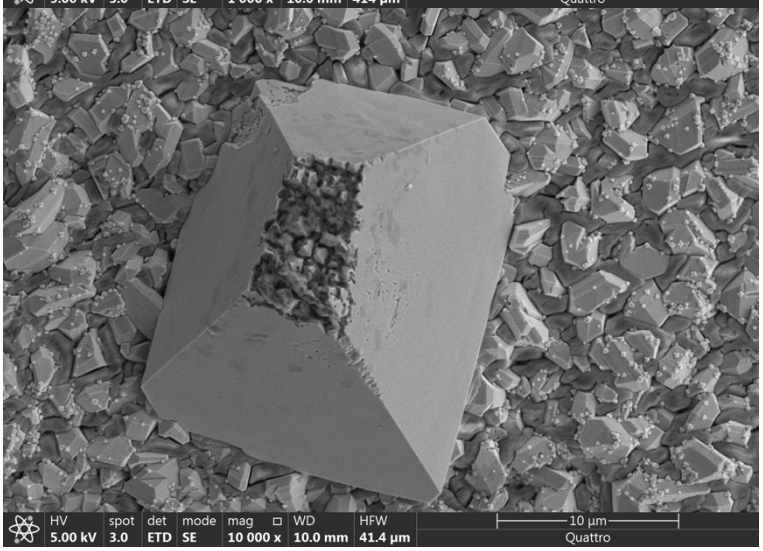

Figure 46 SEM images of unpenetrated part of positively cellulose nitrate at 25% of limiting current. (a) 250X. (b) 1000X. (c) 10,000X. Please refer to Fig.11(c) for the electrochemical method to obtain this sample

a

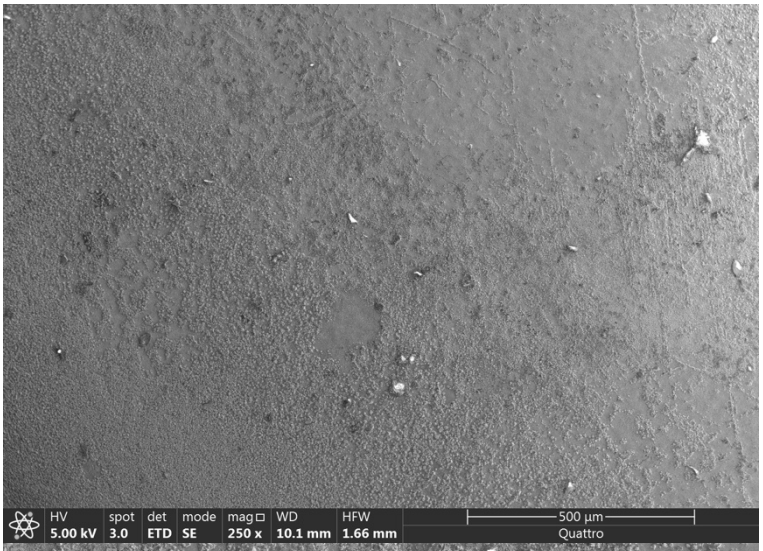

b

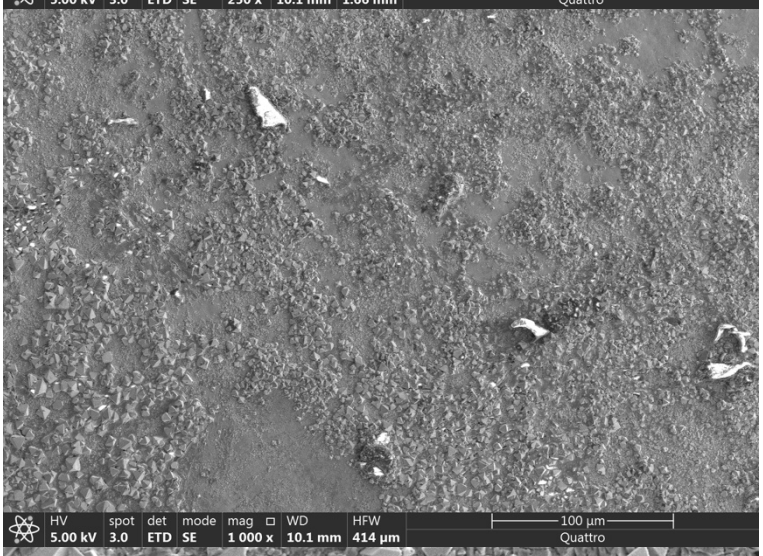

c

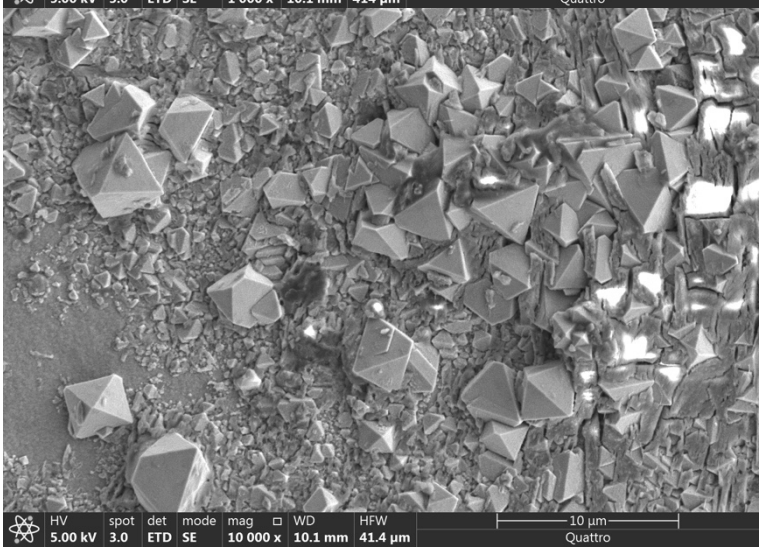

Figure 47 SEM images of unpenetrated part of positively cellulose nitrate at 50% of limiting current. (a) 250X. (b) 1000X. (c) 10,000X. Please refer to Fig.12(c) for the electrochemical method to obtain this sample

a

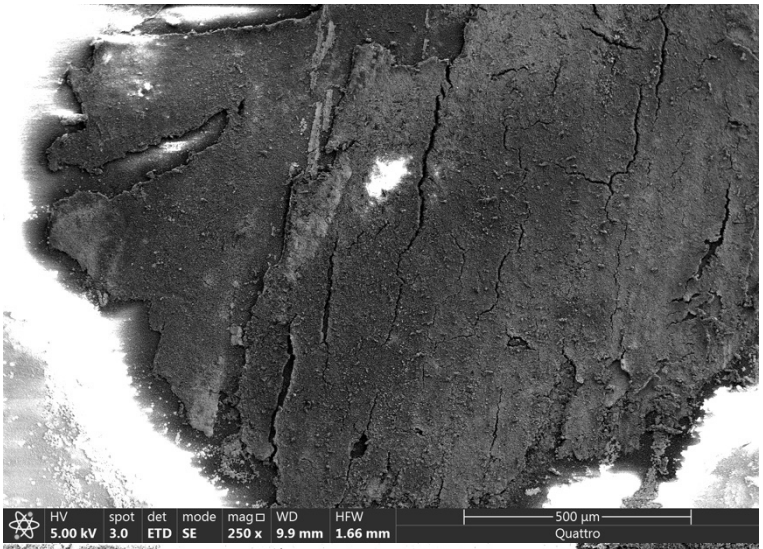

b

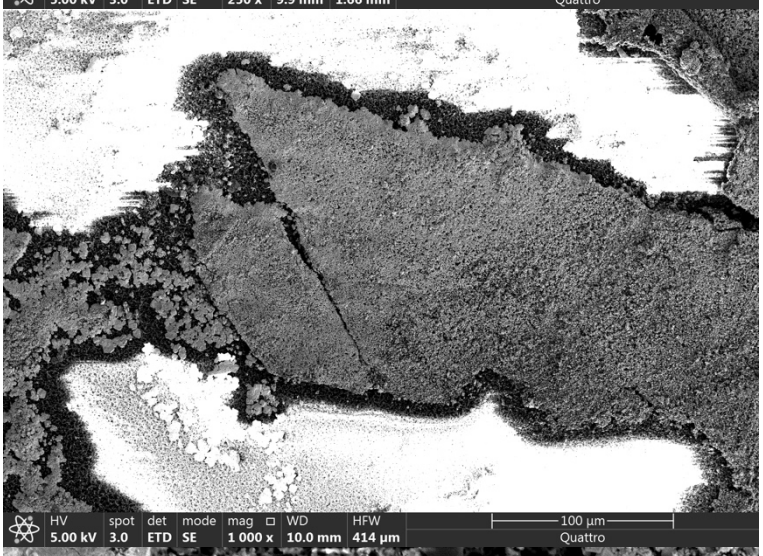

c

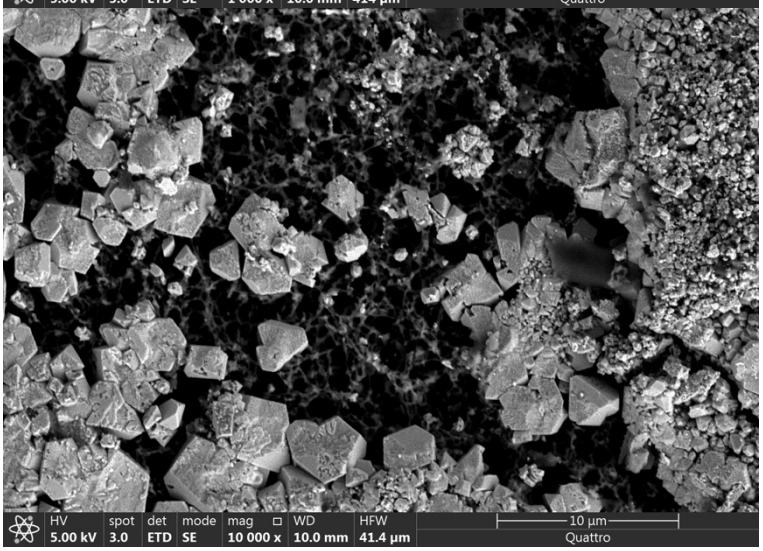

Figure 48 SEM images of penetrated part of positively cellulose nitrate at 10% of limiting current. (a) 250X. (b) 1000X. (c) 10,000X. Please refer to Fig.10(c) for the electrochemical method to obtain this sample

a

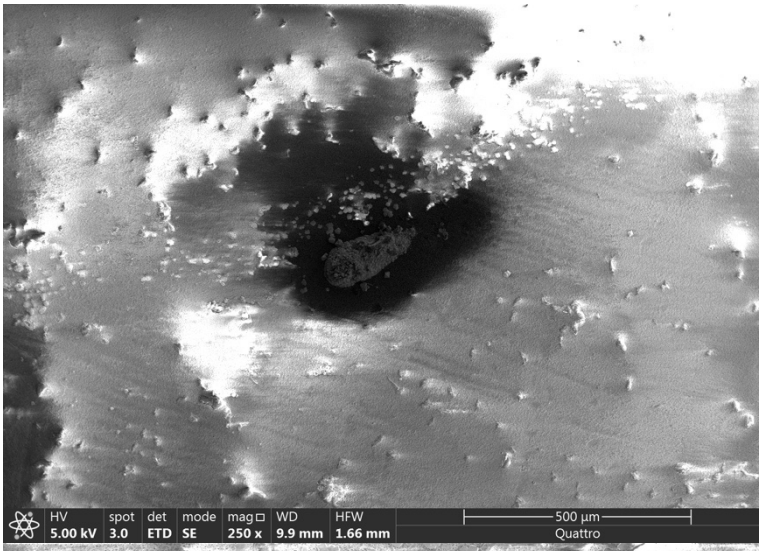

b

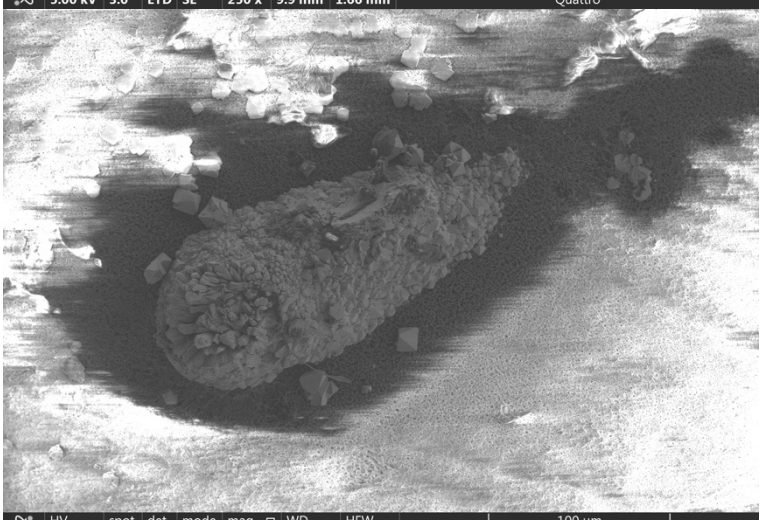

c

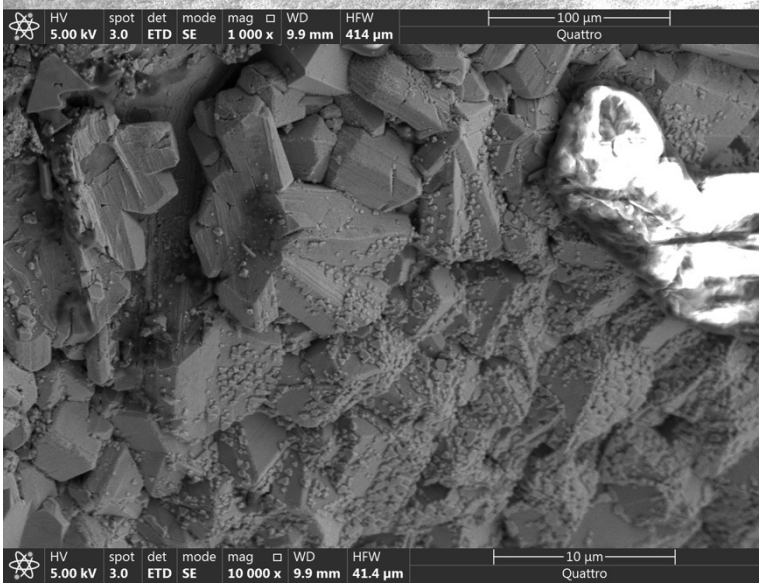

Figure 49 SEM images of penetrated part of positively cellulose nitrate at 25% of limiting current. (a) 250X. (b) 1000X. (c) 10,000X. Please refer to Fig.11(c) for the electrochemical method to obtain this sample

a

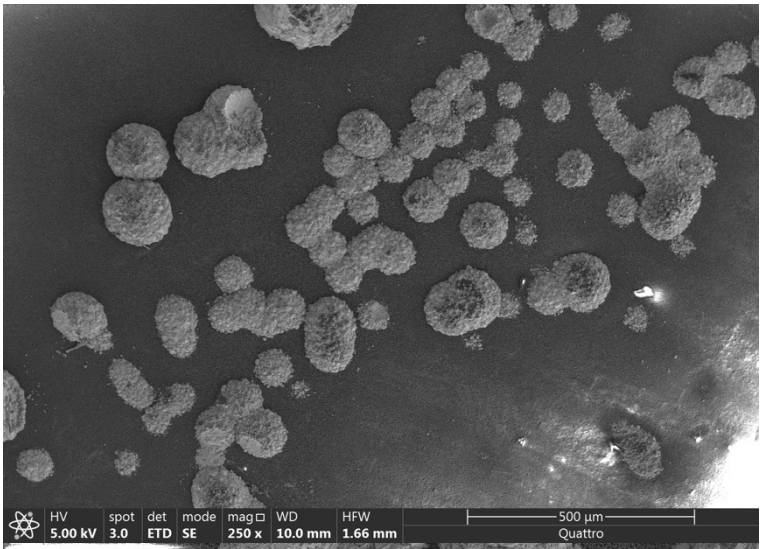

b

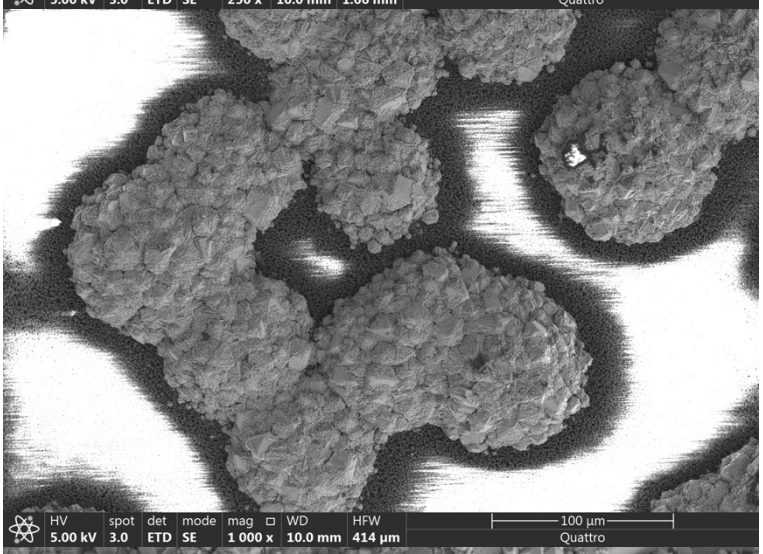

c

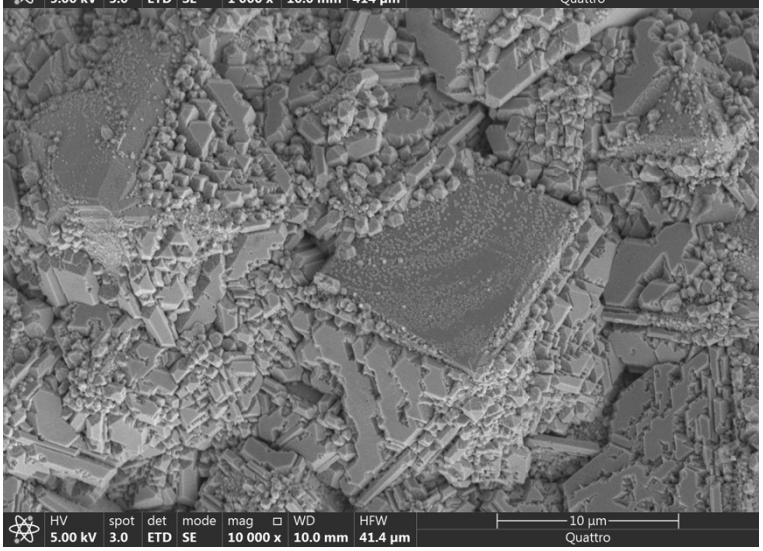

Figure 50 SEM images of penetrated part of positively cellulose nitrate at 50% of limiting current. (a) 250X. (b) 1000X. (c) 10,000X. Please refer to Fig.12(c) for the electrochemical method to obtain this sample

Chapter 5: Conclusion and Future Directions

The mechanisms and performance of modified separators in dilute electrolytes and at over-limiting current conditions reported in recent studies inspired us to explore the fundamental science for the modified separators in practically concentrated electrolytes and at under-limiting current conditions While we expect that positively charged pores will have better performance, due to the localization of flux, the negatively charged pores turned out to outperform the positively charged ones in terms of the penetration capacity.

In the linear sweep voltammetry part, we can tell that with concentration raises, the surface charge effect is reduced. For separators with large pore size (cellulose nitrate), the phenomenon will disappear at low concentration. The separators with small pore size will still have that phenomenon at high concentration. Surface charge effect is strongly affected by the double layer to radius. The chronopotentiometry results indicate that negatively charged separators might have better performance than the positively charged separators in general for ceramic coated and tri-layer PE separators.

Overall, the negatively charged separators have better performance than positively charged ones. Positively charged separators did not always stop the dendrite penetration and that's contradictory with our hypothesis. The possible cause is the depletion area. The negatively charged separators might have larger cation transportation cross-section area than the positively charged ones due to the surface charge effect. When the dendrite starts to grow, the pores with larger deposition cross section area need longer time to grow certain length and that's the reason negatively charge separators will resist longer. The varying degree of the interconnectivity among separator pores may have also played a role that need to be addressed in the future study.

At 25% LC, the negatively charged separators are likely to have the best performance among all percentages of limiting current. Combining with SEM images, we can tell that at 25% LC will likely have more regular primary nucleation and more regular secondary nucleation. When each system is charging with 10% LC, the overall current density is small. Even though some parts may be preferred to have deposition, the local current density is still small, and a few pores can sustain the transportation process. Also, the local potential is also small enough to avoid transport limitation. The 25% LC charging is likely to have local high current density and transport limitation may happen. So that more pores are involved in to ensure the transportation is under critical value. The 50% LC charging is likely to have critical transportation limitations and the potential is too high that drives the dendrite growth into fast speed so that the nucleation is not regular, and penetration happens quickly. The nucleation of 50% LC samples will be irregular and chaotic due to high local current density and transportation limitation happening in the pores. From nucleation perspective, when the deposition happened, copper cation reduced into copper metal on the copper electrode and the energy barrier of nucleation should be very small but due to different surface charge, the interface energy will also influent the nucleation. According to Scharifker-Hills model [23], the nuclei density is calculated as:

$$N = 0.065\sqrt{\left(\frac{1}{8\pi C_0 V_m}\right)} * (\frac{nFC_0}{i_{max}t_{max}})^2$$

In the equation, C_0 is the bulk concentration and V_m is the molar volume of copper. The key parameters in our system are $i_{max}\ and\ t_{max}$. The current is fixed during the chronopotentiometry so the product of $i_{max}\ t_{max}$ is the penetration capacities. From Fig. 13, we can tell that the 25% LC samples for ceramic coated and tri-layer PE trend to have high penetration capacities than 10% LC and 50% LC ones. From the equations, the nuclei density of

25% LC samples should be lower than 10% LC and 50% LC samples and that's uniform with the SEM images for both ceramic coated and tri-layer PE separators.

In the future, AAO and ceramic coated separators will be tested in non-aqueous Lithium/ $LiPF_6$ systems in order to figure out surface charge effect in the commercialized battery systems. And X-ray CT scan will be conducted in order to get the morphology of the dendrite in 3D to get better understanding of the mechanism of dendrite growth.

References

1. Electrochemical Physics for the Precision Engineering of Next-Generation Batteries (P. Bai, 2017)
2. Trasatti, S., 1799–1999: Alessandro Volta's 'Electric Pile': Two hundred years, but it doesn't seem like it. Journal of Electroanalytical Chemistry, 1999. **460**(1): p. 1-4.
3. Yao, N.P., C.C. Christianson, and F. Hornstra, Prospect of advanced lead-acid, nickel/iron and nickel/zinc batteries for electric vehicle applications. 1981.
4. Whittingham, M.S., Electrical energy storage and intercalation chemistry. Science, 1976. **192**(4244): p. 1126-1127.
5. Xu, W., et al., Lithium metal anodes for rechargeable batteries. Energy & Environmental Science, 2014. **7**(2): p. 513-537.
6. Nikonenko, V. et al. (2010). Intensive current transfer in membrane systems: Modelling, mechanisms and application in electrodialysis. Adv. Colloid Interface Sci. 160, 101–123
7. Andersen, M. B. et al. (2012). Current-induced membrane discharge. Phys. Rev. Lett. 109, 108301
8. Han, J.-H., Khoo, E., Bai, P. & Bazant, (2014). M. Z. Over-limiting current and control of dendritic growth by surface conduction in nanopores. Sci. Rep. **4,** 7056.
9. Han, J.-H., Wang, M., Bai, P., Brushett, F. R., & Bazant, M. Z. (2016) Dendrite Suppression by Shock Electrodeposition in Charged Porous Media. Scientific Reports, **6**(1).
10. Mani, A., Zangle, T. & Santiago, J. (2009). On the propagation of concentration

polarization from microchannel-nanochannel interfaces Part I: analytical model and characteristic analysis. Langmuir 25, 3898–3908.

11. Zangle, T., Mani, A. & Santiago, J. (2009). On the propagation of concentration polarization from microchannel-nanochannel interfaces Part II: numerical and experimental study. Langmuir 25, 3909–3916.
12. Yaroshchuk, A., Zholkovskiy, E., Pogodin, S., & Baulin, V. (2011). Coupled Concentration Polarization and Electroosmotic Circulation near Micro/Nanointerfaces: Taylor–Aris Model of Hydrodynamic Dispersion and Limits of Its Applicability. Langmuir, **27**(18)
13. Zhang, S. S., Xu, K., & Jow, T. R. (2006).Charge and discharge characteristics of a commercial LiCoO2-based 18650 Li-ion battery. Journal of Power Sources, **160**(2), 1403–1409.
14. Owen, M. J., & Smith, P. J. (1994). Plasma treatment of polydimethylsiloxane. Journal of Adhesion Science and Technology, **8**(10), 1063–1075.
15. Hegemann, D., Brunner, H., & Oehr, C. (2003) Plasma treatment of polymers for surface and adhesion improvement. Nuclear Instruments and Methods in Physics Research Section B: Beam Interactions with Materials and Atoms, **208**, 281–286.
16. Nitschke, M., Schmack, G., Janke, A., Simon, F., Pleul, D., & Werner, C. (2001) Low pressure plasma treatment of poly(3-hydroxybutyrate): Toward tailored polymer surfaces for tissue engineering scaffolds. Journal of Biomedical Materials Research, **59**(4), 632–638.

17. Greenwood, O. D., Boyd, R. D., Hopkins, J., & Badyal, J. P. S. (1995).Atmospheric

silent discharge versus low-pressure plasma treatment of polyethylene, polypropylene, polyisobutylene, and polystyrene. Journal of Adhesion Science and Technology, **9**(3), 311–326.

18. Yuri Lvov, Katsuhiko Ariga, Izumi Ichinose, and Toyoki Kunitake. (1995) Journal of the American Chemical Society **117** (22), 6117-6123
19. SU, B., Wang, T., Wang, Z., Gao, X., & Gao, C. (2012). Preparation and performance of dynamic layer-by-layer PDADMAC/PSS nanofiltration membrane. Journal of Membrane Science, 423-424, 324–331.
20. Ali, M., Yameen, B., Cervera, J., Ramírez, P., Neumann, R., Ensinger, W., … Azzaroni, O. (2010). Layer-by-Layer Assembly of Polyelectrolytes into Ionic Current Rectifying Solid-State Nanopores: Insights from Theory and Experiment. Journal of the American Chemical Society, **132**(24), 8338–8348.
21. Nagaura, T, (1990). Lithium ion rechargeable battery. Progress in Batteries & Solar Cells, **9**: p. 209.
22. An, S. J., Li, J., Daniel, C., Mohanty, D., Nagpure, S., & Wood, D. L. (2016). The state of understanding of the lithium-ion-battery graphite solid electrolyte interphase (SEI) and its relationship to formation cycling. Carbon, **105**, 52–76.
23. Grujicic, D., & Pesic, B. (2002). Electrodeposition of copper: the nucleation mechanisms. Electrochimica Acta, **47**(18), 2901–2912.